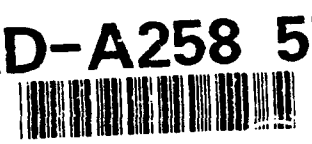

1. AGENCY USE ONLY (Leave blank)	2. REPORT DATE	3. REPORT TYPE AND DATES COVERED
	1992	THESIS/~~DISSERTATION~~

4. TITLE AND SUBTITLE

Satellite Derived Rainfall and the Intensity of Tropical Cyclones and Possible Relationships to Sea Surface Temperature

5. FUNDING NUMBERS

6. AUTHOR(S)

Timothy D. Hutchison, Captain

7. PERFORMING ORGANIZATION NAME(S) AND ADDRESS(ES)

AFIT Student Attending: St Louis University

8. PERFORMING ORGANIZATION REPORT NUMBER

AFIT/CI/CIA- 92-106

9. SPONSORING/MONITORING AGENCY NAME(S) AND ADDRESS(ES)

AFIT/CI
Wright-Patterson AFB OH 45433-6583

10. SPONSORING/MONITORING AGENCY REPORT NUMBER

11. SUPPLEMENTARY NOTES

12a. DISTRIBUTION/AVAILABILITY STATEMENT

Approved for Public Release IAW 190-1
Distributed Unlimited
ERNEST A. HAYGOOD, Captain, USAF
Executive Officer

12b. DISTRIBUTION CODE

13. ABSTRACT *(Maximum 200 words)*

14. SUBJECT TERMS	15. NUMBER OF PAGES 88
	16. PRICE CODE

17. SECURITY CLASSIFICATION OF REPORT	18. SECURITY CLASSIFICATION OF THIS PAGE	19. SECURITY CLASSIFICATION OF ABSTRACT	20. LIMITATION OF ABSTRACT

DISCLAIMER NOTICE

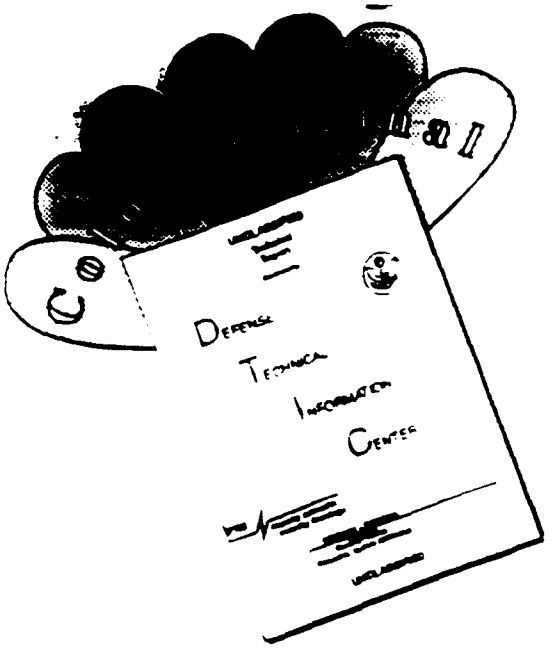

THIS DOCUMENT IS BEST QUALITY AVAILABLE. THE COPY FURNISHED TO DTIC CONTAINED A SIGNIFICANT NUMBER OF COLOR PAGES WHICH DO NOT REPRODUCE LEGIBLY ON BLACK AND WHITE MICROFICHE.

Hutchison, Timothy D., Capt, USAF, 1992: **SATELLITE DERIVED RAINFALL AND THE INTENSITY OF TROPICAL CYCLONES AND POSSIBLE RELATIONSHIPS TO SEA SURFACE TEMPERATURE.** 88 pp, Master of Science, St. Louis University.

ABSTRACT

This research used a nonlinear algorithm developed by Olson, et al. (1989) to retrieve rainrates from satellite derived microwave brightness temperatures for tropical cyclones over tropical oceanic regions. These derived rainrates were used to determine the total 24 hour rainfall and subsequent, amount of energy generated via latent heat release for eight cases. The results showed good agreement with previous results and indicate that the SSM/I is a useful tool in assessing the total amount of rainfall of a tropical cyclone over oceanic regions.

The derived rainrates were used to determine total rainfall, total convective rainfall and total stratiform rainfall. These were correlated with surrounding sea surface temperatures. Results indicate there is only a weak correlation between sea surface temperatures and the convective, stratiform and total rainfall. This supports previous findings regarding the highly complex nature of tropical cyclones and the nonlinearity of the numerous predictors. Stronger correlations were found between the sea surface temperature variance and rainfall indicating that the temperature contrast may be more important in determining rainfall than the actual temperatures.

Significantly stronger relationships were identified between sea surface temperature and storm intensity. Strong correlations were found between SST's surrounding the storm and the future intensity. The most significant relationship was found for the outer regions and the intensity 24-48 hours later which agrees with the 1-2 day lag between convective bursts and intensification. It seems apparent that SST's play a critical role in this process, although the specific mechanism is not known.

SATELLITE DERIVED RAINFALL AND THE INTENSITY OF TROPICAL CYCLONES AND POSSIBLE RELATIONSHIPS TO SEA SURFACE TEMPERATURE

Timothy D. Hutchison, B.A.

A Digest Presented to the Faculty of the Graduate School of Saint Louis University in Partial Fulfillment of the Requirements for the Degree of Master of Science (Research)

1992

DIGEST

This research used a nonlinear algorithm developed by Olson, et al. (1989) to retrieve rainrates from satellite derived microwave brightness temperatures for tropical cyclones over tropical oceanic regions. These derived rainrates were used to determine the total 24 hour rainfall and subsequent, amount of energy generated via latent heat release for eight cases. The results showed good agreement with previous results and indicate that the SSM/I is a useful tool in assessing the total amount of rainfall of a tropical cyclone over oceanic regions.

The derived rainrates were used to determine total rainfall, total convective rainfall and total stratiform rainfall. These were correlated with surrounding sea surface temperatures. Results indicate there is only a weak correlation between sea surface temperatures and the convective, stratiform and total rainfall. This supports previous findings regarding the highly complex nature of tropical cyclones and the nonlinearity of the numerous predictors. Stronger correlations were found between the sea surface temperature variance and rainfall indicating that the temperature contrast may

be more important in determining rainfall than the actual temperatures.

Significantly stronger relationships were identified between sea surface temperature and storm intensity. Strong correlations were found between SST's surrounding the storm and the future intensity. The most significant relationship was found for the outer regions and the intensity 24-48 hours later which agrees with the 1-2 day lag between convective bursts and intensification. It seems apparent that SST's play a critical role in this process, although the specific mechanism is not known.

SATELLITE DERIVED RAINFALL AND THE INTENSITY OF TROPICAL CYCLONES AND POSSIBLE RELATIONSHIPS TO SEA SURFACE TEMPERATURE

Timothy D. Hutchison, B.A.

A Thesis Presented to the Faculty of the Graduate School of Saint Louis University in Partial Fulfillment of the Requirements for the Degree of Master of Science (Research)

1992

COMMITTEE IN CHARGE OF CANDIDACY:

Professor Gandikota V. Rao,
Chairperson and Advisor

Assistant Professor Charles P. Graves

Associate Professor James T. Moore

ACKNOWLEDGEMENTS

I would like to take this opportunity to thank several people who have offered their assistance during the research and preparation of this thesis. First, Prof. Gandikota V. Rao, my graduate research advisor, provided valuable guidance and support and was instrumental in the completion of this research. I would also like to thank Prof. James T. Moore for his assistance in the initial stages of the computer processing and his valuable discussions and Prof. Charles Graves for his input and assistance. Mr. Eric Haug and Kevin Hutcheson (no relation) at the St. Louis University Department of Earth and Atmospheric Sciences who provided immeasurable computer assistance, without which this research would have been thwarted early on. Mr. Gerald Felde at the Air Force Geophysics Laboratory provided the SSM/I data and software for processing. My opportunity to pursue the Master of Science was sponsored by the Air Force Institude of Technology. Finally, I would like to thank my wife, Koryn, whose support, tolerance and encouragement throughout my research was critical in my completion of the master's program.

TABLE OF CONTENTS

Page

LIST OF TABLES

LIST OF ILLUSTRATIONS

CHAPTER 1. INTRODUCTION

Tropical cyclones (i.e. tropical storms, hurricanes or typhoons) cause vast amounts of damage worldwide each year. This damage is caused by strong winds, storm surge and heavy rainfall. Table 1.1 shows a partial damage estimate for several 1987 typhoons. Considerable attention has been placed on the analysis and forecasting of winds in the vicinity of tropical cyclones, while in fact much of the damage is due to the heavy rainfall. One of the costliest hurricanes in U.S. history, Hurricane Agnes (1972), caused $2.1 billion damage due to devastating floods. The torrential rains of Hurricane Camille (1969) caused 150 deaths in the Blue Ridge Mountains of Virginia. Although research efforts have increased recently, rainfall studies are not receiving the attention they deserve. This, in part, is due to the poor rainfall estimation capability over remote oceanic regions.

Prior to 1987, the United States Air Force flew weather reconnaissance missions into tropical cyclones in the North Western Pacific. These missions were ceased in 1987 and the observation of tropical cyclones in remote oceanic regions was relegated to

Table 1.1. List of 1987 typhoons which had significant human costs. Numbers do not include lost time or travel and shipping delays. Figures are from JTWC annual tropical cyclone report.

Storm	Location	Human loss	Material loss
Thelma	Korea	Many dead	Extensive
Wynne	Marianas		Extensive
Alex	Korea	Many dead	Major floods
Betty	Philippines	20–27 dead 60,000 homeless	$millions
Dinah	Japan		$millions
Gerald	Taiwan China	5 dead 122 dead	$millions $millions
Lynn	Taiwan	42 dead 18 missing	$millions
Nina	Truk Atoll Philippines	5 dead 40,000 homeless 687 dead 500,000 homeless	$30–40 x 10^6
Phyllis	Philippines	10–23 dead	

another platform, the meteorological satellite. In 1987, the Defense Meteorological Satellite Program (DMSP) launched the Special Sensor Microwave/Imager (SSM/I) on one of its polar orbiting satellites. The SSM/I provides information previously unavailable to the tropical cyclone forecaster. Prior to 1987, satellite remote sensor observations were limited to the visible and infrared radiation. Although, these satellites provided nearly continuous monitoring of tropical cyclones additional information, such as rainfall and center locations are needed in their diagnosis and prognosis.

The uniqueness of SSM/I is its measurement of microwave radiances at four microwave frequencies. Three of the frequencies are measured in both vertical and horizontal polarization yielding 7 frequency channels. These channels can be used directly to diagnose certain aspects of the atmosphere and can be combined in both linear and nonlinear algorithms to extract information about other environmental parameters such as cloud moisture, liquid water, surface winds and precipitation rate.

The tropical cyclone exists in a complex environment, one composed of nonlinear interactions of many scales. The tropical cyclone's structure and

lifecycle are dependent on upper and lower level winds, vertical wind profile, and boundary layer processes. For example, sea surface temperature (SST) has been linked to tropical cyclone genesis and maintenance. Several researchers have found a "critical" SST of 26.5C necessary to fulfill the energetics requirements of the developing and intensifying tropical cyclone. However, direct links between tropical cyclone rainfall and the environmental (SST) have not been established.

This research utilizes the SSM/I derived rainrates to study various aspects of a tropical cyclone and its interaction with the boundary layer, specifically the SST's.

An estimation of the total rainfall within a tropical cyclone is also of significance because of the severity of damage it can cause. This study will use the derived rainrates to determine total 24-h rainfall and the consequent latent heat release.

The study will also investigate the relationship between convective, stratiform and total rainfall of a tropical cyclone and SST's within and outside of the cyclone's domain. In addition, it will investigate the relationship between SST and future intensity.

CHAPTER 2. REVIEW OF RELATED LITERATURE

The tropical cyclone (also called tropical storm, hurricane and typhoon) causes vast amounts of destruction as it approaches and makes landfall. It's structure, energetics and motion have been investigated by many researchers for decades. Meteorological satellites provide good spatial and temporal coverage of tropical cyclones enabling a thorough study of their structure. Such studies identified a tropical cyclone to be a complex weather system heavily influenced by and influencing the environmental conditions.

Climatological studies have found that cyclogenesis is dependent on several physical parameters; convective instability, middle level relative humidity, low level cyclonic vorticity, vertical shear of the horizontal wind, and SST and the depth of warm water (Gray, 1979). Of these, the SST has long been considered one of the critical parameters for genesis. Palmen(1948) was the first to mention 26.5C or 80F as a critical SST. Since that time, much research has been done on the importance of SST but the "threshold" has not changed. More recently, Holliday and Thompson (1979) found that SST plays an important

role in the rapidly intensifying hurricane. They found warm water (i.e. >28C) to be necessary, but not sufficient for rapid intensification.

Additional studies have found that SST provides an upward boundary on the tropical cyclone's intensity (potential intensity), but that most never reach this intensity due to the influence of other atmospheric conditions (Merrill, 1987; Merrill, 1988). For example, upper tropospheric environmental flow has been found to be an important determinant (Sadler, 1976) as well the as storm's interaction with the Tropical Upper Tropospheric Trough (TUTT). In addition, Merrill found that there was less vertical shear for intensifying hurricanes and the azimuthal radial outflow tended to be stronger than that of nonintensifying storms.

Although researchers agree that SST is a factor in the tropical cyclone structure and energetics, the degree of this influence has been debated. Frank (1984) investigated the sensible heat budget of the mature hurricane and found the net flux from sea to air in the cyclone core was relatively small (on the order of 50 W m^{-2}). Numerical simulations have shown the importance of both latent and sensible heat flux from the sea surface. For example, Ooyama(1969)

showed only a weak vortex developed when sea surface evaporation was turned off.

Likewise, Emmanuel(1986) hypothesized that the intensification and maintenance of a tropical cyclone depends exclusively on the self-induced heat transfer from the ocean. He showed that a tropical cyclone can be maintained without any contribution from ambient conditional instability.

The precipitation characteristics of the mature hurricane has been investigated by numerous researchers. Miller (1958) examined the rainfall of 16 Florida hurricanes using rain gauges and found a strong asymmetry in the rainfall rates ahead of the storm when compared to those in the rear and found weak right/left asymmetries. He also calculated total 24 hour rainfall using the mean areal rainrates and concluded the average hurricane produced 6.0×10^{19} Joules day^{-1} due to release of latent heat.

More recently, Jorgensen (1984) identified three predominant precipitation features; the eyewall, the stratiform region adjacent to and outside the eyewall, and rainbands which contain both convective and stratiform regions. Further studies have found that variations in the areal averaged rainrates of the

eyewall region were caused by the growth and decay of convective areas (Burpee and Black, 1989). They also found that the distribution of precipitation was asymmetric in both the eyewall and the rainband regions.

This rainfall has been linked to intensification by many investigators. Rodgers and Adler(1981) suggested that a trend of increasing latent heat release(LHR) via precipitation condensation provides an early indication of tropical cyclone intensification. Specifically, they found a 1-2 day lag between peak LHR and maximum tropical cyclone intensity. MacArthur (1991) found that peaks in mean rainfall correlated strongly with the filling or deepening of the storm. He also identified the region within 222-444km of the storm's center as a critical region in which the latent heat released by precipitation results in a corresponding decrease in central pressure.

Gentry et al., (1980) found that cloud top temperatures over the inner core are well correlated with future intensity (24 hour maximum sustained winds). Likewise, Steranka et al. (1986) linked cloud top temperatures and the intensity of the tropical cyclone. They found that convective surges near the

eye, i.e., within 222 km precede the increase of maximum winds. His work also supported the 24-h lag time which agrees with the theoretical relationship between LHR and kinetic energy generation.

Dvorak (1984) developed a technique of diagnosing storm intensity using satellite infrared and visible data by combining both pattern recognition and an objective assessment of cloud top temperatures. It is this technique which satellite analysts at the Joint Typhoon Warning Center (JTWC) use to determine tropical cyclone intensity from satellite data. The positions and intensities of the tropical cyclones used in this study were obtained from the JTWC (Hoffman et al., 1988).

In recent years, microwave data has been found to provide new information regarding the tropical cyclone structure due to its different frequency measuring capabilities compared to IR and visible. Wilheit and Chang (1977) used data from the Electrically Scanning Microwave Radiometer (ESMR) on the Nimbus 5 satellite and found that brightness temperature measurements at 19.35 GHz and 37.0 GHz can be interpreted in terms of rainrate with an accuracy of a factor of 2 over the 1-25 mm h^{-1} range. Rodgers and Adler (1981) also used ESMR-5 microwave data and

showed that brightness temperatures increased as rainrate increased. The data also highlighted inward moving rainbands with intensification, i.e., a consolidation of convection in the core.

Data from the Defense Meteorological Satellite Program's Special Sensor Microwave Imager (SSM/I) has been compared to Visible and IR data in diagnosing the tropical cyclone structure by Glass and Felde(1989) and Velden et al., (1989). They showed that the SSM/I data was better at depicting convective cells in the hurricane especially when they are covered by upper level cirrus. They found particular usefulness of the 85 GHz frequency in identifying well organized rainbands.

Wilheit and Chang (1977) and Spencer et al. (1989) confirmed the usefulness of higher frequency microwave data in identifying rain areas. They found volume scattering by the precipitation, specifically scattering by ice, was the basis of this identification. They also concluded that lower frequencies such as 19 GHz exhibit warming in rain areas which coincide with the higher frequency cooling.

Likewise, Adler et al., (1990) used aircraft microwave observations to observe deep tropical convection and found the ice scattering is the determinant factor effecting the measured microwave radiance with the amount of scattering increasing as frequency increased. Higher frequencies, 18 GHz and 37 GHz especially, exhibit low brightness temperatures in response to the ice in the thunderstorm's middle layers. Figure 2.1 shows a plot of TB's as measured by aircraft when passing over a deep convective core. Notice the dramatic difference between the responses of the IR frequency (11 m) and that of the microwave frequencies (>18 GHz) as the sensor passes over the convection. The largest response is by the higher frequencies (92 and 183 GHz).

Many researchers have composited the above information to develop various rainfall retrieval techniques. Kummerow et al.. (1990) used a multichannel statistical approach to retrieve rainfall rates from TB's obtained from a cloud radiative model and found good agreement with observed rainrates.

Olson et al. (1990) regressed the brightness temperatures against observed rainfall rates in a stepwise multiple linear regression procedure for both midlatitude and tropical scenarios. He found the 85

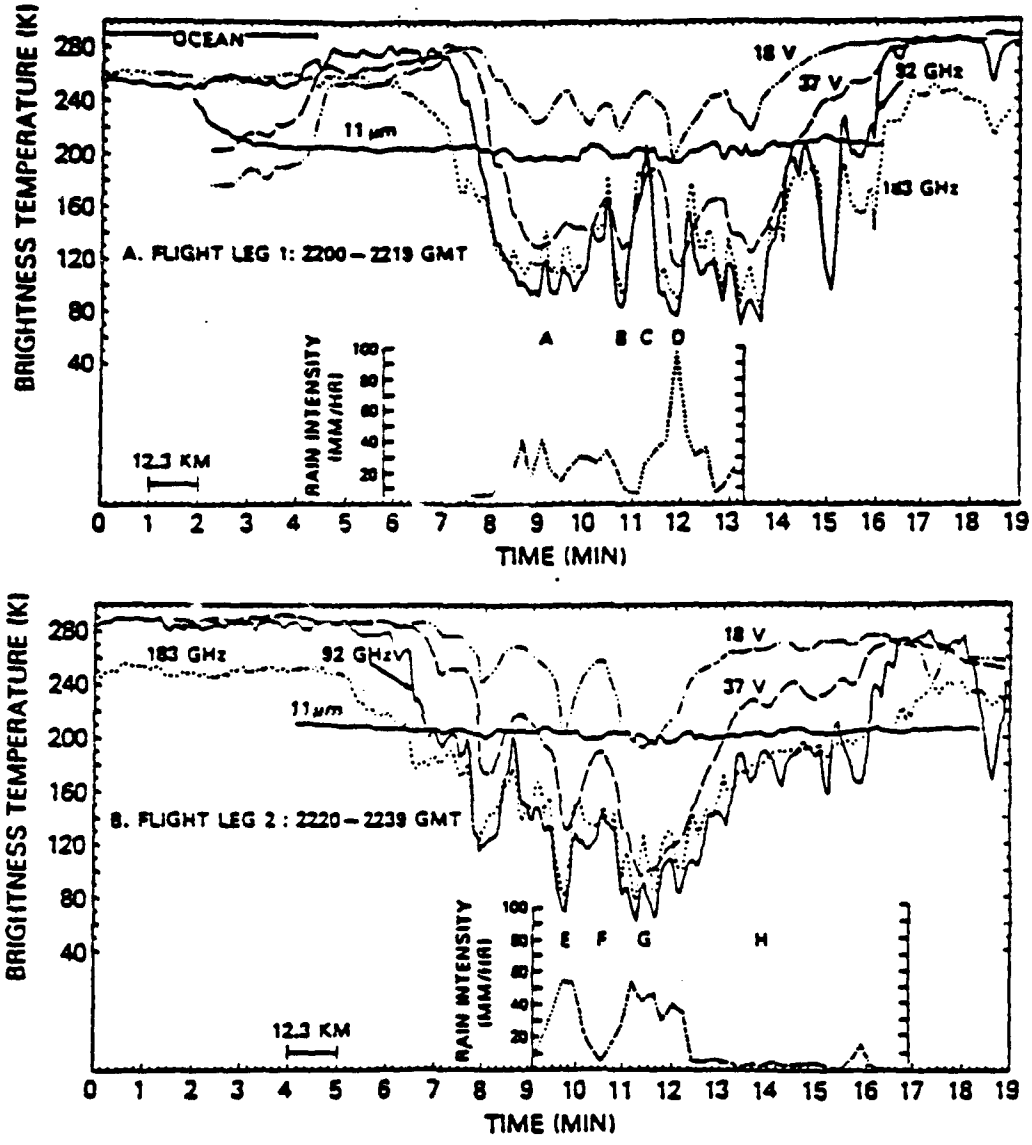

Fig. 2.1 Two aircraft flight tracks over a tropical thunderstorm complex showing the response of several microwave frequencies and one infrared frequency (after Adler et al.,1990)

GHz channel to be the first channel selected in the regression. A more indepth discussion of Olson's algorithm is found in the next chapter. This research will use rainrates derived from Olson's algorithm.

It is apparent from the above discussion, that the microwave observations from the SSM/I provide valuable information for diagnosing rainfall patterns of tropical cyclones. This research will study the rainfall and its relationship to the observed SST's. It will also examine the effect of SST's on the cyclone development.

Chapter 3. BACKGROUND ON MICROWAVE IMAGING

3.1 The Special Sensor Microwave/Imager (SSM/I)

In 1987, the first SSM/I was launched aboard the Defense Meteorological Satellite Program (DMSP) F8 spacecraft. The SSM/I is a joint Air Force/Navy program designed to obtain global observation of atmospheric and surface composition through observation of upwelling microwave radiance from the earth-atmosphere system.

The F8 travels in a circular sun synchronous ascending orbit. This means that it crosses the equator ascending from south to north at the same local time each day. For the F8, this time is 0612 Local Standard Time. The satellite travels at 6.58 km s^{-1} at altitude of 833 km with an inclination of 98.8 degrees. It has an orbital period of 102 minutes and completes 14.1 revolutions per day.

The SSM/I sensor is mounted on the aft of the spacecraft (with respect to the direction of satellite travel). It senses down at a 45 degree angle, thus viewing a region on the earth that is approximately 1200km. This view is behind that viewed by the Operating Line Scanner(OLS) on the F8. The SSM/I has a circular scan with a period of 1.9 seconds, scanning

left to right. It collects data through 102 degrees of the rotation, producing an effective data swath of 1394 km (Fig. 3.1) (Hollinger, 1987).

The sun-synchronous orbit combined with the data swath result in the 24-h global coverage seen in Fig. 3.2. Black regions indicate regions not viewed by the sensor. Since the launch of a second SSM/I mounted on the F10 satellite, these "black out" regions have been reduced substantially. The effect of this coverage on tropical cyclone observation was discussed in Velden et al., (1989). He found that with one SSM/I there was a 89% chance of being observed at least once and 44% chance of being observed twice during a given 24 hour period. A second sensor increases these values substantially to 99% and 89% respectively.

3.2 Microwave Radiation Transfer Properties

When a satellite born microwave sensor measures upwelling microwave radiance, it measures two types; emitted and scattered, both coming from the entire Earth-Atmosphere system. As this radiation passes through the atmosphere, it is attenuated via absorption and scattering by atmospheric constituents. This radiance is measured in terms of brightness temperature.

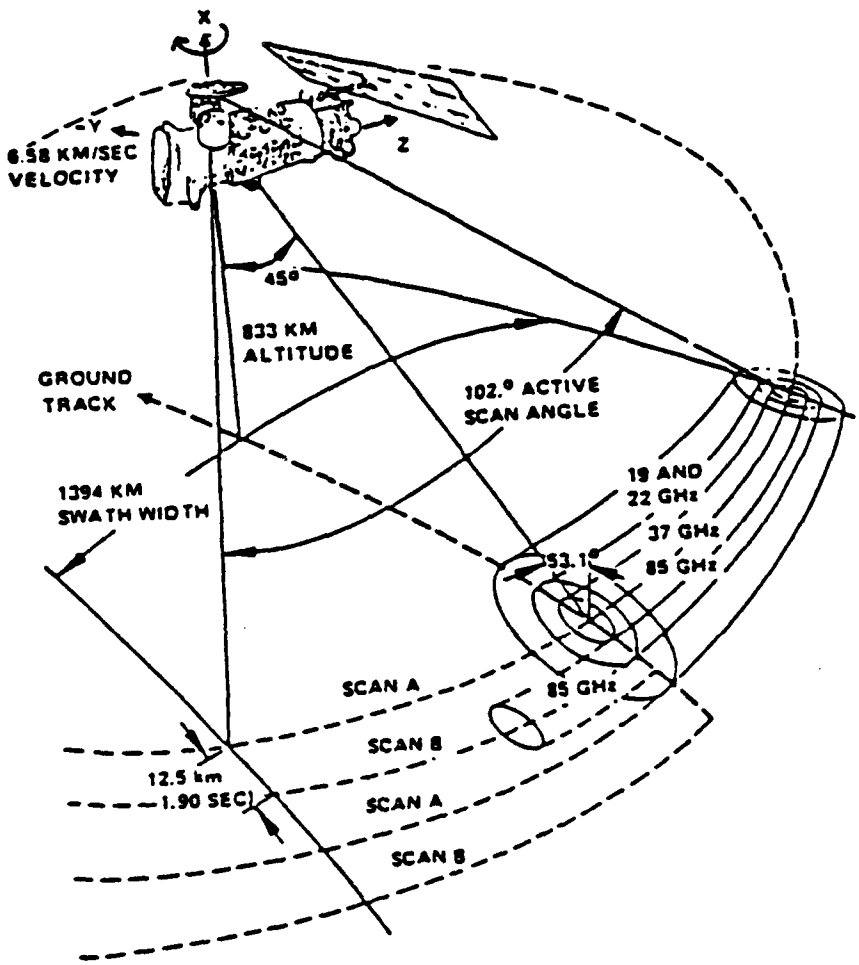

Fig. 3.1 Scan geometry of the SSM/I radiometer. The satellite travels in the direction marked "ground track". The sensor views 1200km behind the subpoint of the satellite. (after Hollinger et al., 1987)

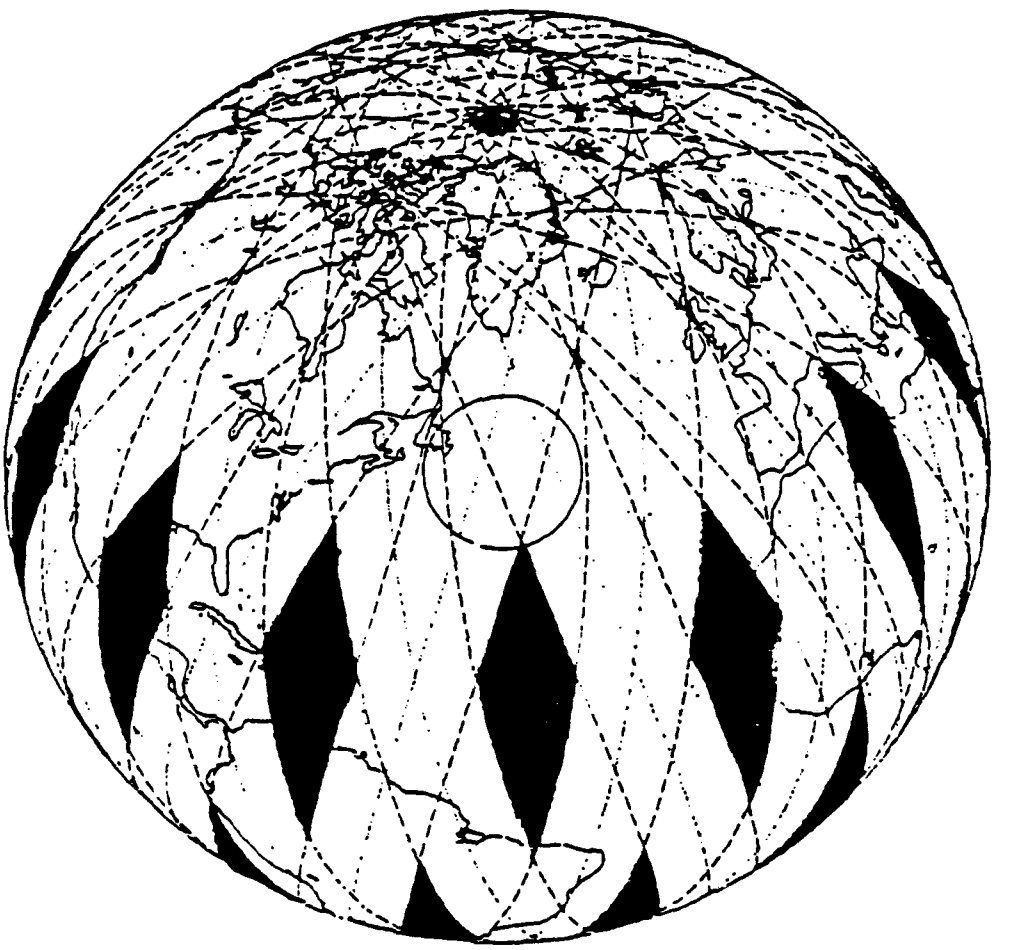

Fig. 3.2. SSM/I 24-hour coverage. Black areas denote regions not viewed by the sensor during the period and are caused by a combination of the polar orbit and the data swath size (after Velden et al., 1990)

In radiative transfer theory, the intensity of the upwelling microwave radiance (B) is a function of the temperature of the radiation source. Thus, the radiance can be represented by its Planck function (in the frequency domain):

$$B_v(T)=2hv^3/[c^2(e^{hv/KT}-1)] \qquad (1)$$

where h represents Planck's constant, v represents frequency, c is the speed of light, K is Boltzmann's constant and T is the temperature. For the microwave frequency range, $hv/KT<<1$, so this relationship can be approximated by

$$B_v(T)\simeq(2Kv^2/c^2)T \qquad (2)$$

Thus, the Planck function, $B_v(T)$, is linearly proportional to the temperature. This relationship is known as the Rayleigh-Jeans law and is valid for a true "blackbody". For a non-black emitter, define the equivalent brightness temperature (TB) so that

$$I_v = (2Kv^2/c^2)TB(v) \qquad (3)$$

where I_v denotes the radiance of a non-black body at frequency v and a brightness temperature of TB. Since the blackbody emits perfectly and the nonblack body

does not, the relationship between the actual radiance I_V and the Planckian radiance, B_V, is represented by the emissivity, $\mathcal{E}$, where

$$\mathcal{E} = - (I_V/B_V) \text{ or } -(TB/T) \quad (4)$$

therefore,

$$TB = \mathcal{E}T \quad (5)$$

The emissivity of the body depends on its composition and physical characteristics (Liou, 1980)

As was stated earlier, the SSM/I sensor measures upwelling radiance from the earth-atmosphere system and converts them to brightness temperatures by a calibration to near-blackbody and cold space radiances. These brightness temperatures are transmitted to ground stations on the earth in the form of Sensor Data Records (SDR) for processing and storage. It is these SDRs which are used in this research to derive the rainrate.

3.3 The Data

The SSM/I is a seven channel, four frequency linearly polarized, passive microwave radiometer. It measures atmospheric and surface microwave brightness

temperatures at 19.35, 22.35 37.0 and 85.5 GHz. It measures horizontal and vertically polarized radiation for all frequencies except 22.35 GHz, thus yielding 7 channels.

Due to the 6.58 km s^{-1} orbital speed of the F8 and the period of the rotating sensor, each SSM/I scan is separated by 12.5 km. In each scan, i.e. both A and B scans, 128 discrete uniformly spaced radiometric samples (pixels) are taken at the two 85 GHz channels, while at alternate scans, i.e. the B scans, 64 discrete samples are taken for the other 5 channels (Fig. 3.1 and Fig. 3.3) (Hollinger et al.,1987). As can be seen, the 85 GHz has a 12.5 km resolution between pixels, while the other channels have a resolution of 25 km.

The actual measuring accuracy of the sensor is better defined by the effective field of view (EFOV) which takes into account both the spatial resolution of sampling and the beamwidth of the radiometer when projected onto the earth's surface (Fig. 3.3). The EFOV is composed of an along track and a cross track contribution. The EFOV is inversely proportional to the frequency, with 85 GHz channels having the smallest EFOV (15km X 13km) and the 19.35 GHz having the largest (69km x 43km)(See Table 3.1). Therefore,

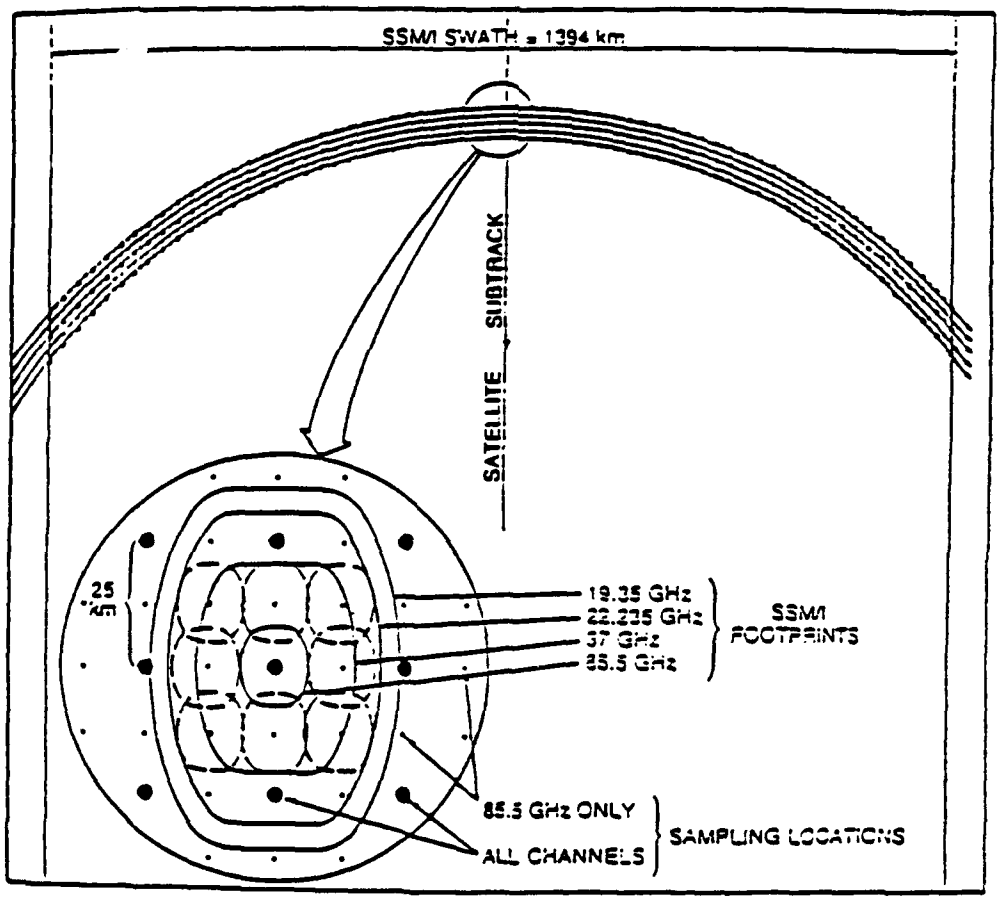

Fig. 3.3. The SSM/I swath coverage and footprints of the various channels. Note that all channels are sampled at the heavy black dots with a spacing of 25 km (called A Scans). Only the 85GHZ is sampled at the smaller dots (called B Scans) (after Spencer et al.,1989)

Table 3.1. List of SSM/I channel characteristics, including frequency, polarization, and Effective Fields of View (EFOV).

Frequency (GHz)	Pol	Beamwidth EFOV (degree)	Surface EFOV	
			Along track (km)	Cross track (km)
19.35	V	1.93	69	43
19.35	H	1.93	69	43
22.235	V	1.83	50	40
37.0	V	1.27	37	28
37.0	H	1.31	37	29
85.5	V	0.60	15	13
85.5	H	0.60	15	13

the sensor actually measures the average microwave emission in the footprint (Hollinger et al., 1987). This averaging can cause an error by as much as a factor of two in the retrieved rainrate and is termed beamfilling. Beamfilling introduces a systematic error when the radiometers field of view is not filled with a uniform rainrate. Techniques are being developed to estimate this effect which incorporates the location of the freezing level, the percentage of the FOV which is raining and the average rainrate within the FOV (e.g. Graves, 1992).

In order to appreciate and interpret the information obtained from the SSM/I data, it is essential to understand the processes which effect the upwelling radiance as it traverses the atmosphere. The microwave radiation originates initially from the earth's surface. In our studies, we are concentrating primarily on oceanic emissions.

As this radiation passes through the atmosphere it is affected by both atmospheric constituents and atmospheric conditions via two processes; absorption and scattering. The constituents that are most radiatively active are water vapor, liquid water (below the freezing level), supercooled water droplets, ice crystals and oxygen. The degree of

impact depends on the size and distribution of the liquid and ice hydrometeors suspended in the atmosphere.

Figure 3.4 shows a plot of the volume scattering and absorption coefficients as well as the single scatter albedo for several microwave frequencies measured by the SSM/I. Scattering is inversely related to frequency, with higher frequencies, such as 85 GHz, being scattered more than lower frequencies. This is expected based on Mie scattering theory. Ice has a single scatter albedo near 1 for all frequencies. Therefore, the presence of ice will result in diminished TBs at all frequencies, but the largest effect will be seen at 85 GHz. In the presence of rain, TBs initially increase at all frequencies. However, with continued increase, higher frequencies begin to decrease as the effects of scattering become dominant. This is particularly noticeable at 85 GHz which saturates at very low rainrates (Spencer et al.., 1989).

Upwelling radiance at 19 GHz is most dependent on the amount of rain below the freezing level and radiance at 85 GHz is most affected by ice above the freezing level (Spencer et al., 1989; Prabhakara et al., 1991). Lower frequencies, such as 19 GHz, are

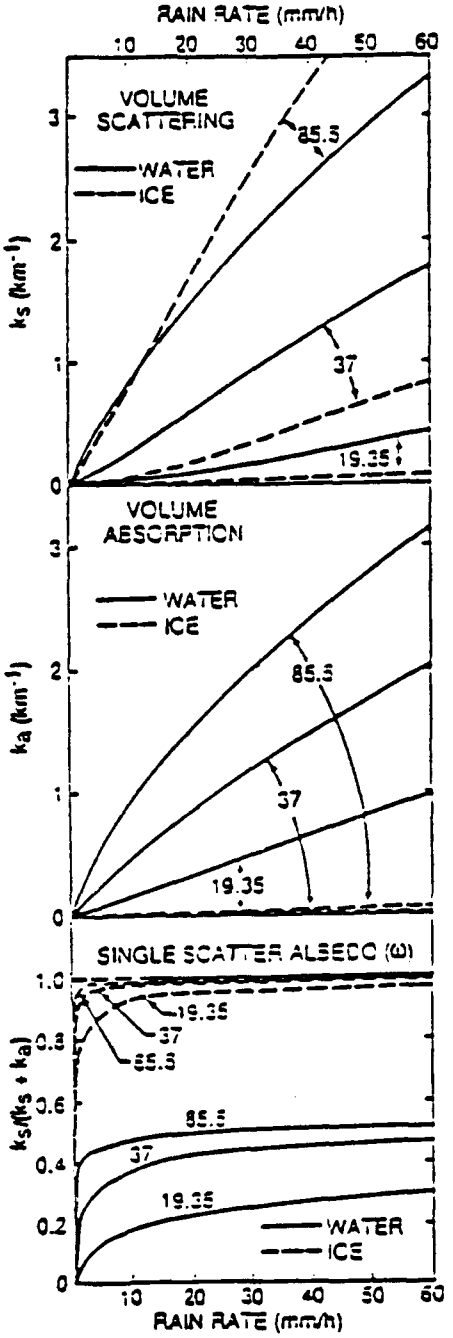

Fig. 3.4. (a) water and ice Mie volume scattering coefficient for 19.35, 37, and 85.5GHZ (b) water and ice volume absorption coefficients for same frequencies (c) ice and water scatter albedos for same frequencies (after Spencer et al.,1989)

minimally affected by scattering and absorption. Thus, this 19 GHz radiation, emitted by low level rain, is able to pass through the atmosphere relatively unhindered and TBs can be used to deduce rain areas and rates.

Rain also emits strongly at frequencies near 37 GHz. This radiation is only marginally affected by scattering of ice found above the rain clouds and can be used to identify rain areas. At higher frequencies, such as 85 GHz, extinction due to absorption and scattering out of the sensor's EFOV significantly affect the radiation and no direct information can be concluded regarding the rain below. Scattering based retrieval techniques rely on the 85 GHz cooling in the presence of deep convection to obtain rainrates. (Spencer et al.,1989; Adler et al., 1990). However, this property causes deep convection to appear cold and enables the depiction of cirrus-covered convection. Thus it has proven extremely useful in analyzing convective rain bands and the presence of the eyewalls in tropical cyclones (Velden et al., 1989; Lee and Caughey, 1989).

There is a good correlation between 19 GHz TB warming and 85GHz TB cooling in tropical oceanic precipitating systems. Many current retrieval tech-

niques utilize both correlations, i.e., the scattering of higher frequencies and the emission of lower frequencies by rain in determining rainrate.

Figures 3.5 and 3.6 show Hurricane Florence at 00:21UTC on 10 September 1988 just prior to landfall near the Mississippi delta. In particular, Fig. 3.5a shows the 85 GHz horizontally polarized channel. Areas that are yellow and red indicate cold brightness temperatures and depict deep convection within the bands surrounding the hurricane's eye. Likewise, Figure 3.5b shows the 19 GHz vertically polarized channel and identifies the rain region. The 19 GHz emissions from the earth's surface are colder than the emissions by the rain. Therefore, the rain areas appear as warm and are identified by the light purple and red banding areas extending from the coast south into the Gulf of Mexico (Hollinger, 1991).

Olson (1990) developed a nonlinear algorithm using all four frequencies available from the SSM/I by regressing the brightness temperatures against rainfall rates in a stepwise multiple linear regression. The exponential form allows for a better regression fit to the data, since the response of all the SSM/I channels to changes in rainrates diminishes with increasing rate. The algorithm utilizes five of

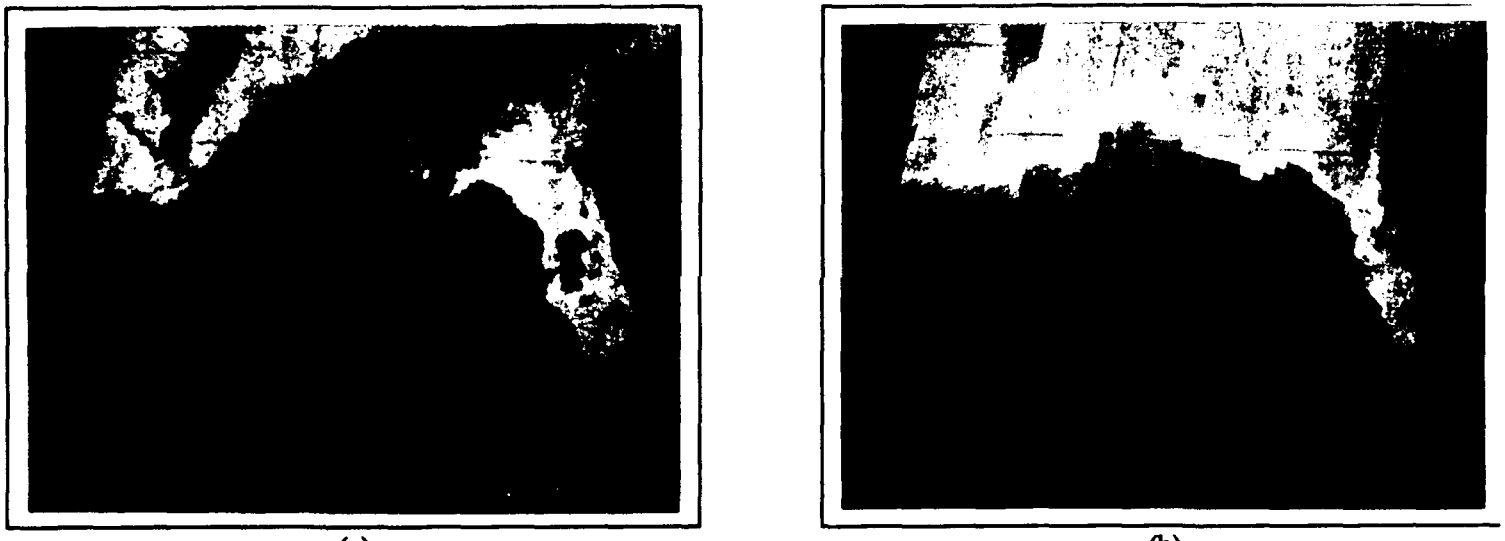

Fig 3.5. (a) 85.5 horizontally polarized brightness temperatures for Hurricane Florence at 00:21 UTC on September 10, 1988 (b) 19.35 vertically polarized brightness temperatures of Hurricane Florence (after Hollinger, 1991)

the channels including the 85 Horizontal and the 19 GHz seen in Fig. 3.5a and 3.5b. Figure 3.6a shows the rainrates retrieved from Olson's algorithm. Notice the spatial distribution and overall pattern along with the quantitative results correlate well with the "ground truth" rainrates obtained from nearby meteorological radar (Fig. 3.6b).

In Olson's algorithm, rainfall rates greater than 5 mm/hr tend to be underestimated, while the majority of rain estimates are within 2 mm/hr of those rain-rates determined from radar information. It is important to note that the SSM/I averaged rain rates are for a 625 km^2 area while that for the radar derived rainrates is roughly 4 km^2 (Hollinger, 1991)

This research uses rainrates derived from Olson's algorithm for all rainfall calculations.

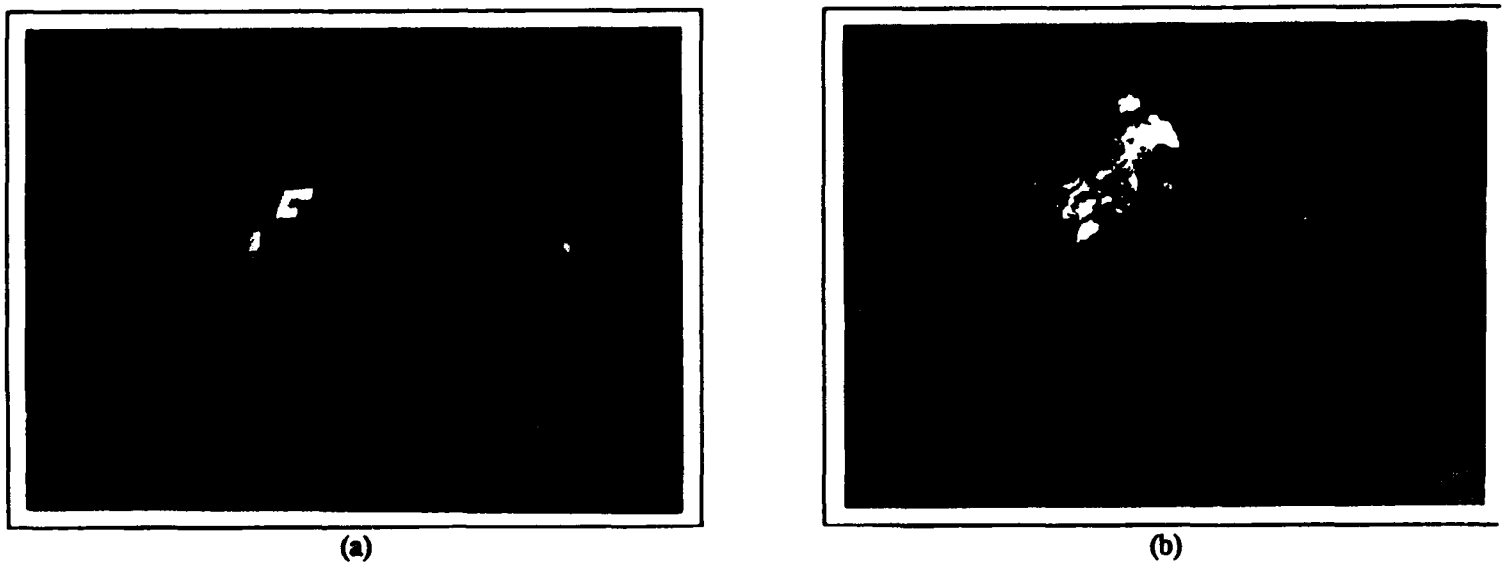

Fig. 3.6. Same as Fig. 3.5, except (a) Rainrates of Florence as determined using Olson et al., algorithm (b) Rainrates as determined from ground-based NWS WSR-57 radar (after Hollinger, 1991)

CHAPTER 4. PROCEDURE/METHODOLOGY

4.1 SSM/I Data Processing

The SSM/I data used in this research was obtained from the archives of the Naval Research Laboratory (NRL) in Washington D.C., through the Air Force Geophysical Laboratory (AFGL) at Hanscom AFB, MA. The data, in the form of Sensor Data Records (SDR's), was loaded onto magnetic tapes at NRL and sent to St. Louis University.

Tropical cyclone positions, intensities and movement were obtained from the Annual Tropical Cyclone Report (Hoffman, et. al., 1987). The positions of all tropical cyclones, i.e., those reaching at least tropical storm intensity were plotted on a large polar stereographic map. Once each storm's track was plotted, F8 orbital information was used to reconstruct each orbit using nodal crossing information obtained from NRL and an orbital wheel to identify specific orbits which having adequate storm coverage (Conway, 1989). (Adequate coverage was determined to be when the satellite subtrack passed within 3 degrees of the tropical cyclone center. If more than 3 degrees, it was assumed that coverage would not include the whole storm system.

Once specific orbits were identified, precise orbital information including nodal crossing time and time-past-ascension hack times were used to determine extraction parameters. Finally, raw SDR data for each chosen orbit was extracted from the magnetic tapes and converted to Mercator projection for further processing using programs from AFGL.

The Mercator grid was a 512 x 300 uniformly spaced seven level grid with 10 km spacing between grid points. Each level corresponded to one of the seven microwave channels. Since 10 km is less than the EFOV of all the SSM/I channels, observed brightness temperatures were interpolated to the grid points, thus filling the grid.

4.2 Rainrate processing

Once in a mercator projection, five of the frequencies were used to derive the rainrates according to the algorithm from Olson et al., (1989). Although, Olson suggested algorithms for both tropical land and tropical oceanic areas only the oceanic algorithm was used, since the data was screened for proximity to or over land locations. This was due to the fact that rainrates in the vicinity of coastline are in-determinable because the measured radiances are

mixture of land and oceanic emissions and cannot be resolved.

In this research, 85GHz data was available for all cases and the algorithm was as follows:

$$R=[\exp(3.06231 - .0056036*85V + .0029478*85H - .0018119*37V - .00750*22V + .0097550*19V) - 8.0] \text{ mm } h^{-1}$$

Although the SSM/I is designed to measure microwave radiances in the 85GHz interval, the sensor on the F8 satellite has lost its capability to measure 85GHz, both vertical and horizontal. Olson developed an alternative algorithm for cases in which 85GHz is not available. It is

$$R=[\exp(5.10196 - .05378*37V + .02766*37H + .01373*19V) - 2.0] \text{ mm } h^{-1}$$

As with the brightness temperatures, derived rainrates were interpolated onto the mercator grid for further processing, thus leading to a spatial "resolution" of 10km. It is important to realize that this is not the true resolution of the rainrates for reasons discussed in the previous section. The actual resolution of the rainrates is approximately 35km.

4.2.1 Total 24 hr Rainfall

Total rainfall was calculated using a similar technique to that used by Miller (1958) except Miller used rain gauge data and calculated areal averages of all hurricanes. This research calculates total rainfall for each individual tropical cyclone and then averages the final values for comparison.

Total rainfall amounts were calculated for all cases with multiple orbits within a 24-h period. Due to the nature of the satellite orbit, time differences between consecutive passes were typically 11.5 to 12.5 hours.

A spatial integration for the 888km x 888km box and a temporal integration for the 24-h period was performed to obtain total rainfall amounts. The spatial integration was accomplished by breaking the large box into 80 smaller 111km x 111km areas (Fig. 4.1), calculating averages for each small area. The average for each box was then integrated forward in time and the rain amounts were summed to yield the total rain.

For example, if two passes were available during a given 24-h period, means were calculated for the 80 boxes for both maptimes. Averages were extrapolated

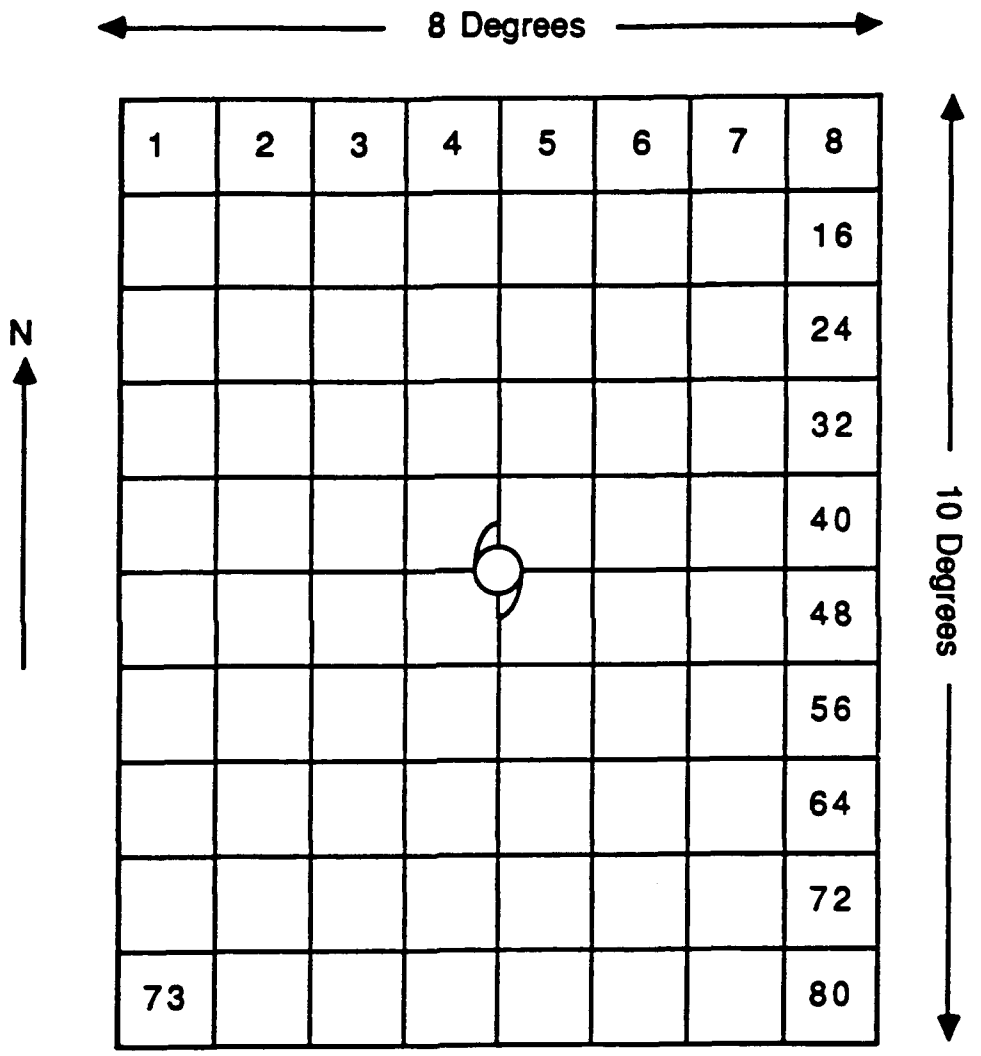

Fig. 4.1. Grid used for the spatial integration used in calculating the total 24 hour rainfall for 888km x 888km box centered on the tropical cyclone

in time to cover the observed period. The total rainfall in the smaller areas were summed yielding the total rainfall over the larger area. Total rainfall was extrapolated to 24 hours if necessary. The amount of latent heat released by condensation was then calculated.

4.2.2 Total, Convective and Stratiform Rainfall Determination

Once in the mercator format, basic statistical calculations were performed on the data to obtain mean, maximum, minimum, standard deviation, variance and the frequency distribution of the rainfall for various radii boxes. Although previous research (McCoy, 1991; MacArthur,1991) divided these boxes into left and right boxes based on direction of movement, this research concentrates on calculations for the entire box (Fig. 4.2). The box was oriented along the direction of typhoon movement as determined from the ATCR. The length of each of the box sides was twice the radius. Thus, a 222km radius box is a box measuring 444km x 444km centered on the tropical cyclone. This study utilized the 222km, 333km and 444km boxes for reasons explained earlier.

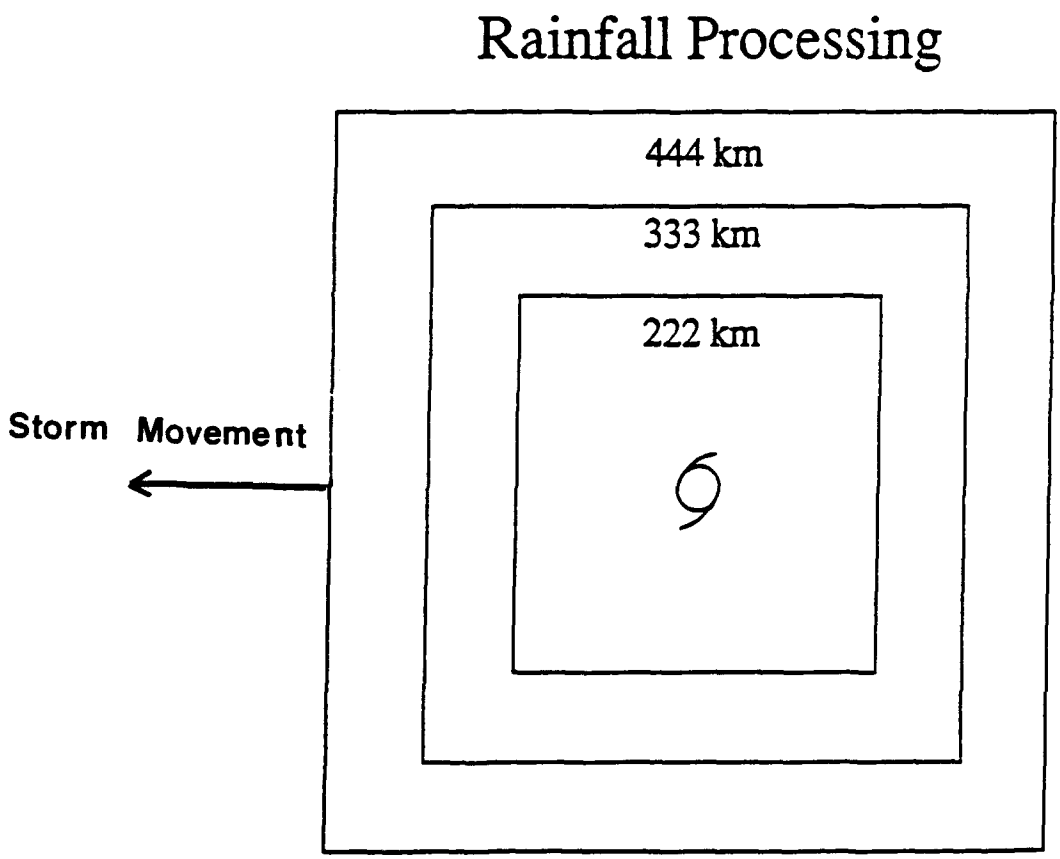

Fig. 4.2. Various areas used for determination of total, total convective and total stratiform rainfall at maptime. The boxes are oriented in the direction of the storm's movement.

Once mean rainrates were obtained, these means were integrated over the area to arrive at the total rainfall per hour over the entire box (mm^3h^{-1}). Likewise, the total convective rainfall per hour was determined by calculating the percentage of rainfall that was convective and multiplying by the total rainfall per hour. Convective rainfall was determined to be rainfall greater than 3.0 mm h^{-1}. This relatively low value was used to take into consideration the large EFOV of the SSM/I channels and is consistent with values used by other researchers. (Willoughby, 1988).

4.3 Sea Surface Temperature (SST) Processing

Sea Surface Temperature data for the North Western Pacific was obtained from the United States Air Force Environmental Tactical Applications Center. The temperatures are part of the Global Surface Temperature Data Base. The sea temperatures are processed at the Fleet Numerical Oceanographic Center in Monterey, CA. and are a combination of ship and satellite reports onto a grid of 100nm resolution. These data are further processed at the Air Force Global Weather Central by further interpolation down to 25nm (46km) and used to produce the global surface temperature database.

This database is an 8th mesh data grid with a spatial resolution of 25 nm and a temperature accuracy within 0.1K. As can be seen by Fig. 4.3, the northern hemisphere is broken up into 64 boxes, each containing 64 x 64 or 4096 grid point. Each grid point within a grid box is specified by an "I" horizontal and a "J" vertical coordinate. Thus, any grid point can be identified by its grid box and its I and J coordinate. (USAFETAC, 1986)

Once particular orbits had been identified for use in the study, SST's were extracted from the database for a 16 x 16 degree square centered on the tropical cyclone. This large box containing SST's was further broken down into 10 smaller areas as shown in Fig. 4.4. These areas include the center box, the northeast, northwest, southeast and southwest quadrants. In addition, in an attempt to investigate the effect of SST's surrounding the cyclone, the outer region was divided into North, South, East and West outer regions.

For the correlations to rainfall, SST's were extracted for the area surrounding the cyclone 24 hours prior to the maptime. This experiment assumes a lag between the time of the encounter of the SSTs and their possible effect on rainfall. Likewise, for the

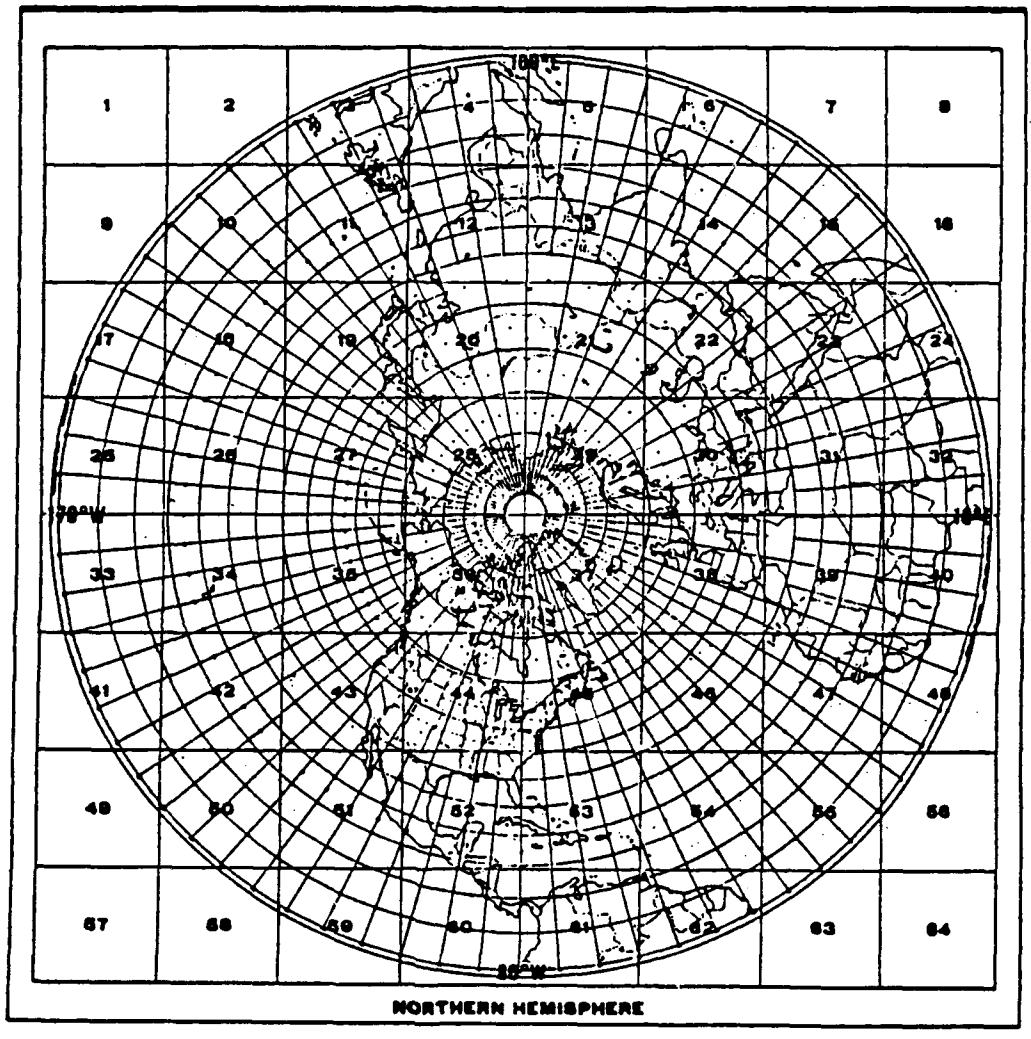

Fig. 4.3. The Eighth Mesh Grid for the Northern Hemisphere used for sea surface temperature extraction from Global Surface Temperature Data Base

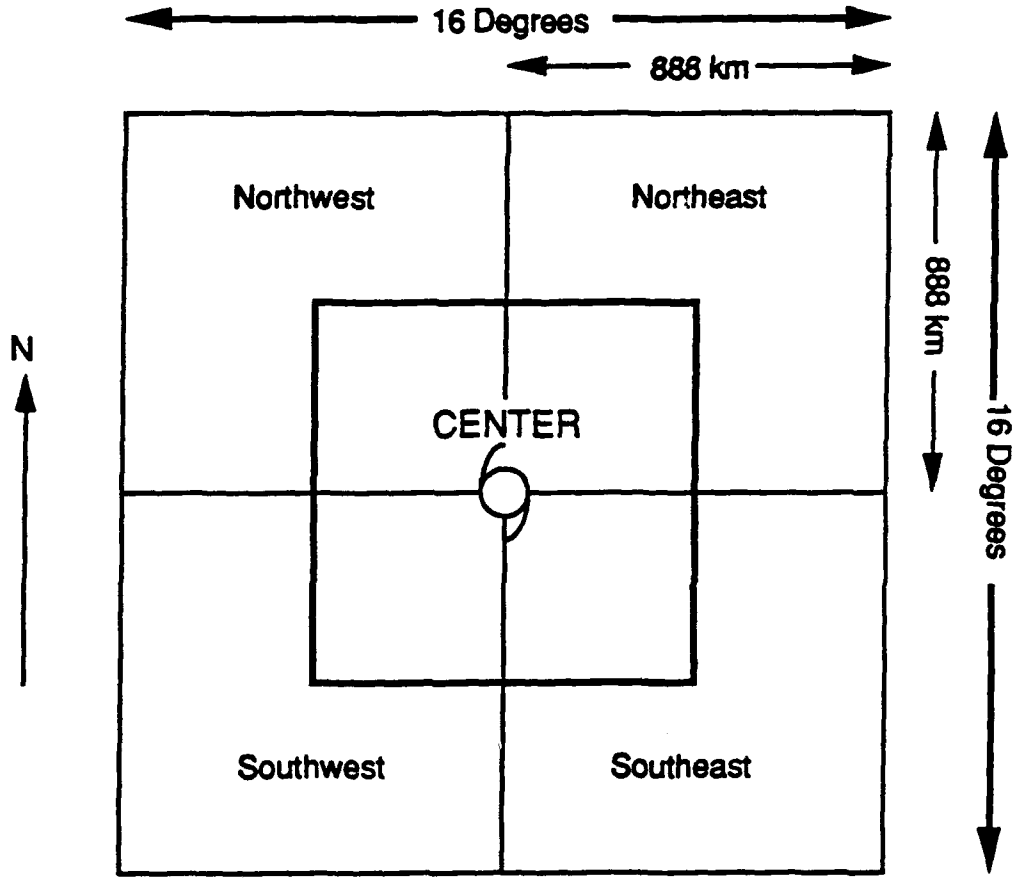

Fig. 4.4. Illustration of sea surface temperature regions extracted for correlation studies. The entire box is 16 degrees (or 1776km) on a side. The center region and the four quadrants are 888km x 888km. The outer region is that region between the outer box and the center region. This outer region was further broken down into North, South, East and West.

intensity correlations, SST's were extracted for the region surrounding the tropical cyclone at the maptime position but 24 hours earlier. This was done because those SSTs at the maptime position and the maptime would be heavily contaminated by the cloud cover. By using SST's 24 hours prior, the assumption was made that remote sensing observations would be more likely and the resulting SST's more accurate. Also, the SSTs could be expected to change little on the large scale in this short of a time span. A schematic showing which SSTs were extracted is seen in Fig. 4.5.

Once SST's were divided into these boxes, the mean, standard deviation and variance were calculated for use in the correlation studies.

4.4 Tropical cyclone intensity

Tropical cyclone intensity can be measured by either the lowest central pressure of the storm or the maximum sustained winds in the core of the storm. For this study, maximum sustained winds were used. Intensities were obtained from the final best track for each maptime as published in the Joint Typhoon Warning Center's Annual Tropical Cyclone Report (Hoffmann et al., 1987). Intensities were obtained for 0, 12, 24, 36 and 48 hours after maptime.

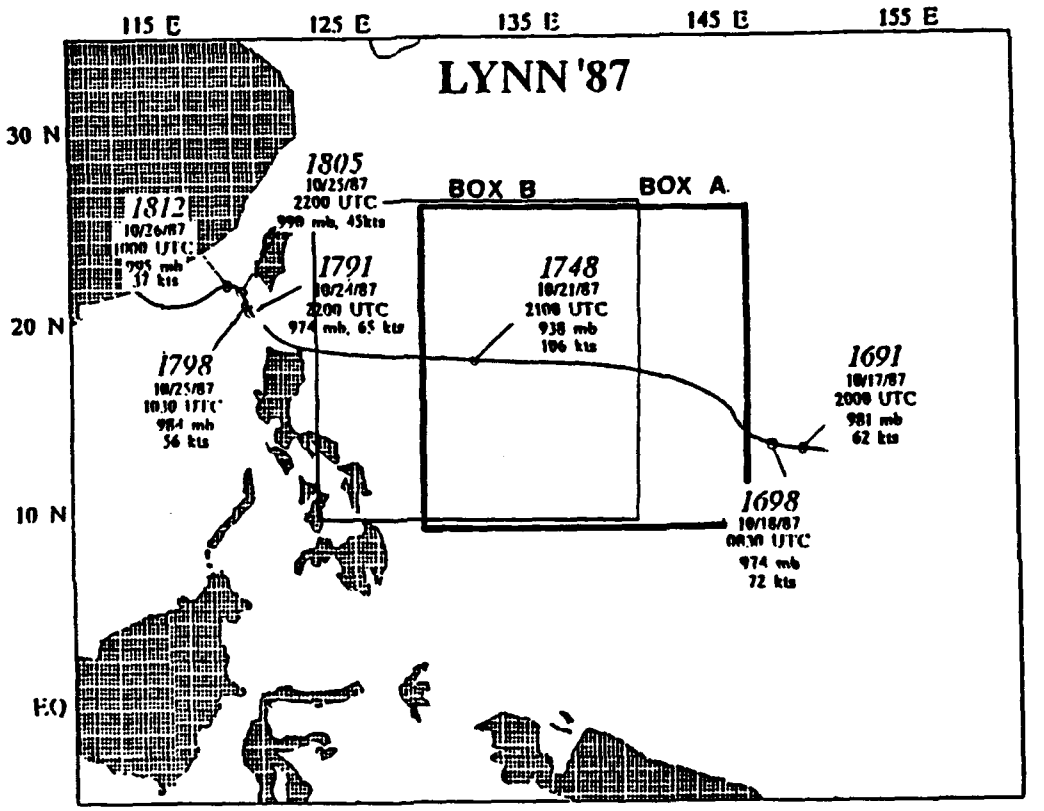

Fig. 4.5. Illustration of the two sea surface temperature cases extracted for the correlation studies. Box A indicates the area surrounding the storm 24 hours earlier. These SST's were used in the rainfall studies. Box B indicates the area surrounding the storm at its current position but 24 hours earlier as discussed in the text. These SST's were used in the intensity correlations.

4.5 Statistical Processing

Once the data was processed, SST's were correlated with the total rainfall, total convective rainfall, total stratiform rainfall and future intensities. Standard linear regression techniques were used. In addition, SST variances were used to examine more precisely the distribution of SST's in the individual boxes and the effect of this variance on rainfall and intensity.

CHAPTER 5. RESULTS

5.1. General

The underlying hypothesis of this research is that SST's in the vicinity of a tropical cyclone will effect its energetics and structure. This effect could be manifested in many ways, two of which are rainfall and future intensity.

5.2. Total Rainfall

By performing both a spatial and temporal integration of consecutive satellite passes, total 24-h rainfall amounts were obtained. The data on hand had eight cases in which at least two satellite passes occurred within 24 hours. Table 5.1 shows the details of these eight cases.

Three of these were viewed at an interval of approximately 12 hours. Two cases were observed three times in 24 hours at an interval of approximately 12 hours. In all cases in which the observational period was less than 24 hours, total rainfall calculated was extrapolated to 24 hours.

Figures 5.1, 5.2 and 5.3 show the rainrate distributions for Typhoon Kelly at three maptimes; 12 Oct 87/2100UTC (orbit 1621), 13 Oct 87/2050UTC (orbit

Tropical Cyclone	DATE-TIME (all 1987)	ORBITS	SSM/I Derived Rainfall in period (x 1E19 mm^3)	Total 24hr Rainfall (x 1E19 mm^3)	Latent Heat Released (x 1E19 Joules/day)
*Dinah	24 Aug 2100Z - 25 Aug 0930Z	929-937	1.07	2.06	5.10
*Dinah	29 Aug 2130Z - 30 Aug 1000Z	1000 - 1007	1.44	2.76	6.89
Holly	9 Sep 0800Z - 10 Sep 0800Z	1148-1162	2.67	2.67	6.67
Kelly	12 Oct 2100Z - 13 Oct 2000Z	1621 - 1635	2.29	2.30	5.75
*Kelly	13 Oct 2000Z - 14 Oct 0930Z	1635-1642	1.06	2.04	5.00
*Lynn	17 Oct 2000Z - 18 Oct 0830Z	1691 - 1698	1.41	2.70	6.80
Lynn	24 Oct 2200Z - 25 Oct 2200Z	1791-1798-1805	2.66	2.66	6.66
Lynn	25 Oct 1030Z - 26 Oct 1000Z	1798-1805-1812	2.32	2.37	5.90
Average	NA	NA	NA	2.44	6.10

Table 5.1. The typhoons and maptimes used in the total 24 hour rainfall calculations and the results. An asterisk (*) denotes a case in which only an approximate 12 hour period was used for the integration. In these cases, the period rainfall was extrapolated to 24 hours.

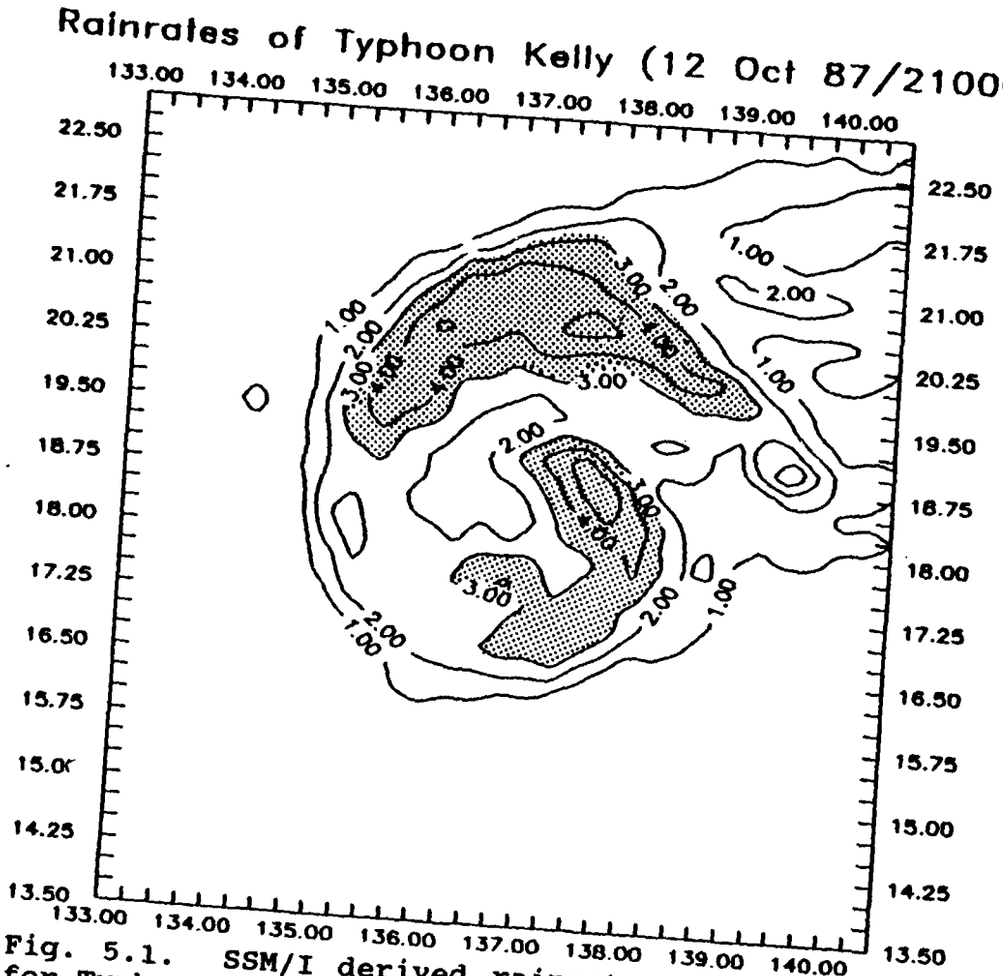

Fig. 5.1. SSM/I derived rainrates using Olson's algorithm for Typhoon Kelly for 12 Oct 1987 at 2100UTC (orbit 1621).

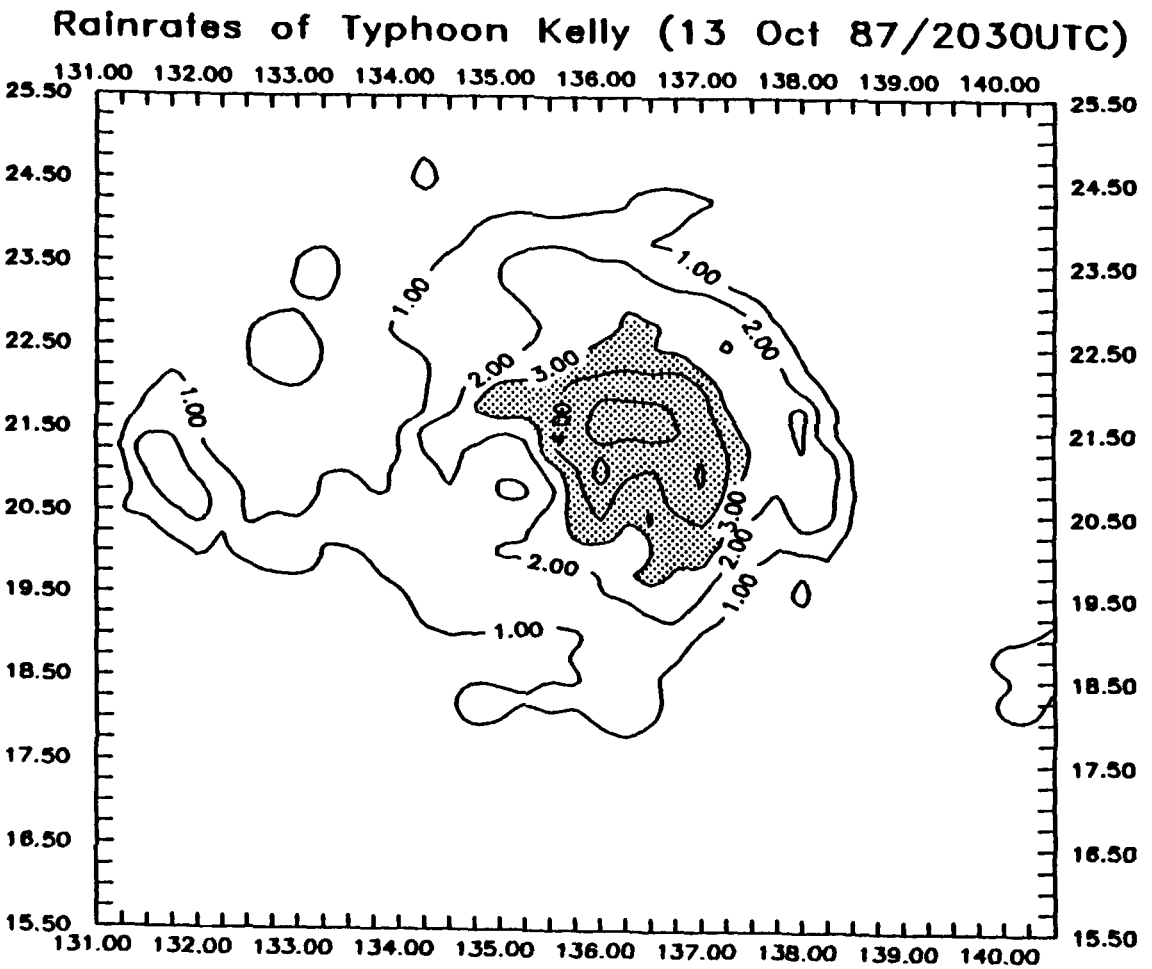

Fig. 5.2. SSM/I derived rainrates using Olson's algorithm for Typhoon Kelly for 13 Oct 1987 at 2030UTC (orbit 1635).

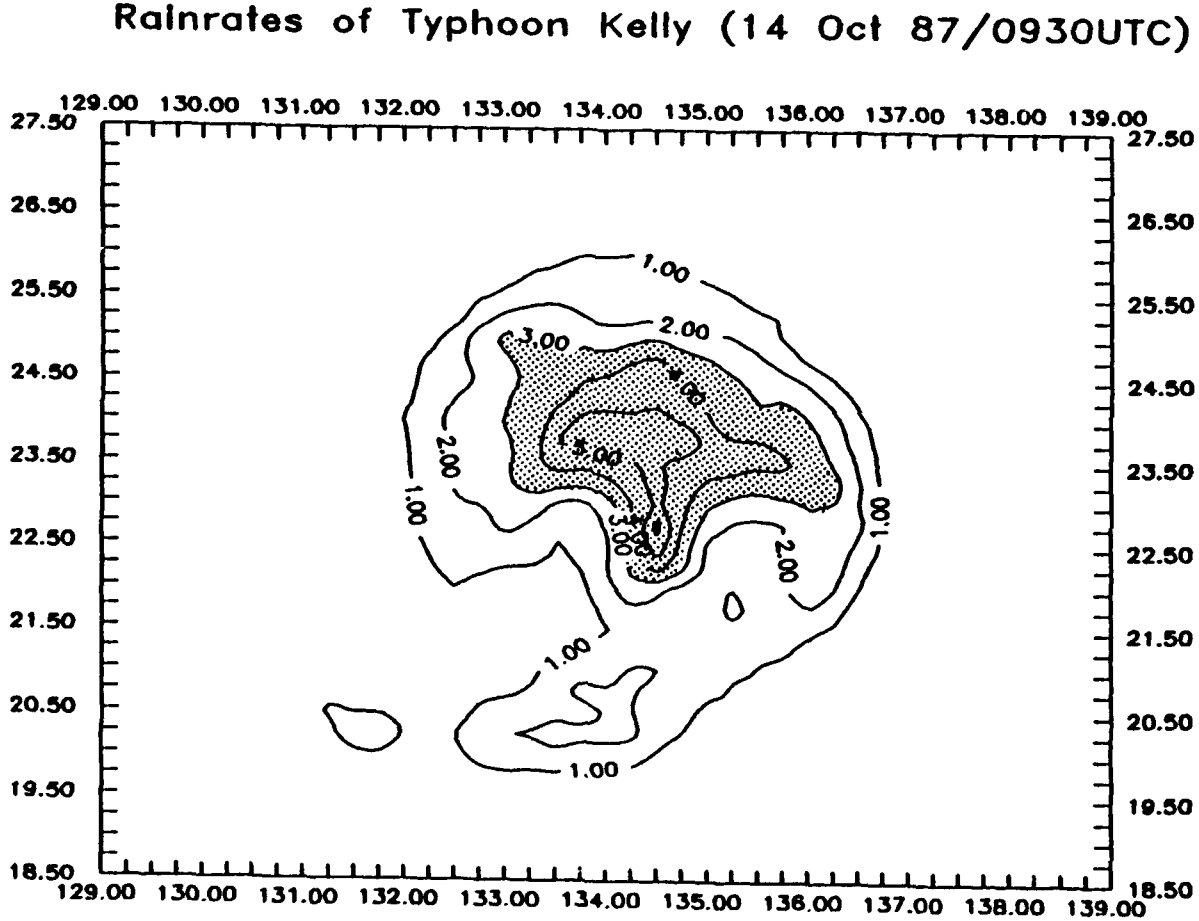

Fig. 5.3. SSM/I derived rainrates using Olson's algorithm for Typhoon Kelly for 14 Oct 1987 at 0930UTC (orbit 1642).

1635) and 14 Oct 87/0930UTC (orbit 1642). These maptimes were some of those used in the total rainfall calculations. Notice how the convective rain areas consolidate in the core region of the storm during intensification, as was observed by Rodgers and Adler (1981). In Fig. 5.1, two convective bands are present, one to the north and one to the southeast. Twenty four hours later, (Fig. 5.2) the convection has begun to consolidate near the core. Further consolidation is evident in Fig. 5.3 (approximately 12 hours later) as the convection intensifies in the core region.

Total rainfall amounts calculated from the areal means are shown in Fig. 5.4. The hatched regions depict the amount out of the total that was extrapolated in order to normalize the total to 24 hours. Total rainfall for the 24 hour period ranged from 1.3 - 2.7 x 10^{19} mm^3 over the 888x888 km box. Latent heat calculations yielded a total energy generation of 3.2-6.9 x10^{19} joules/day (Fig. 5.5). The average value is 6.1 x 10^{19} joules/day. To put this in perspective, this is nearly 10^5 times the total energy of a typical summertime thunderstorm.

Miller(1958) calculated total rainfall using a similar grid for integration, but he used rain gauge

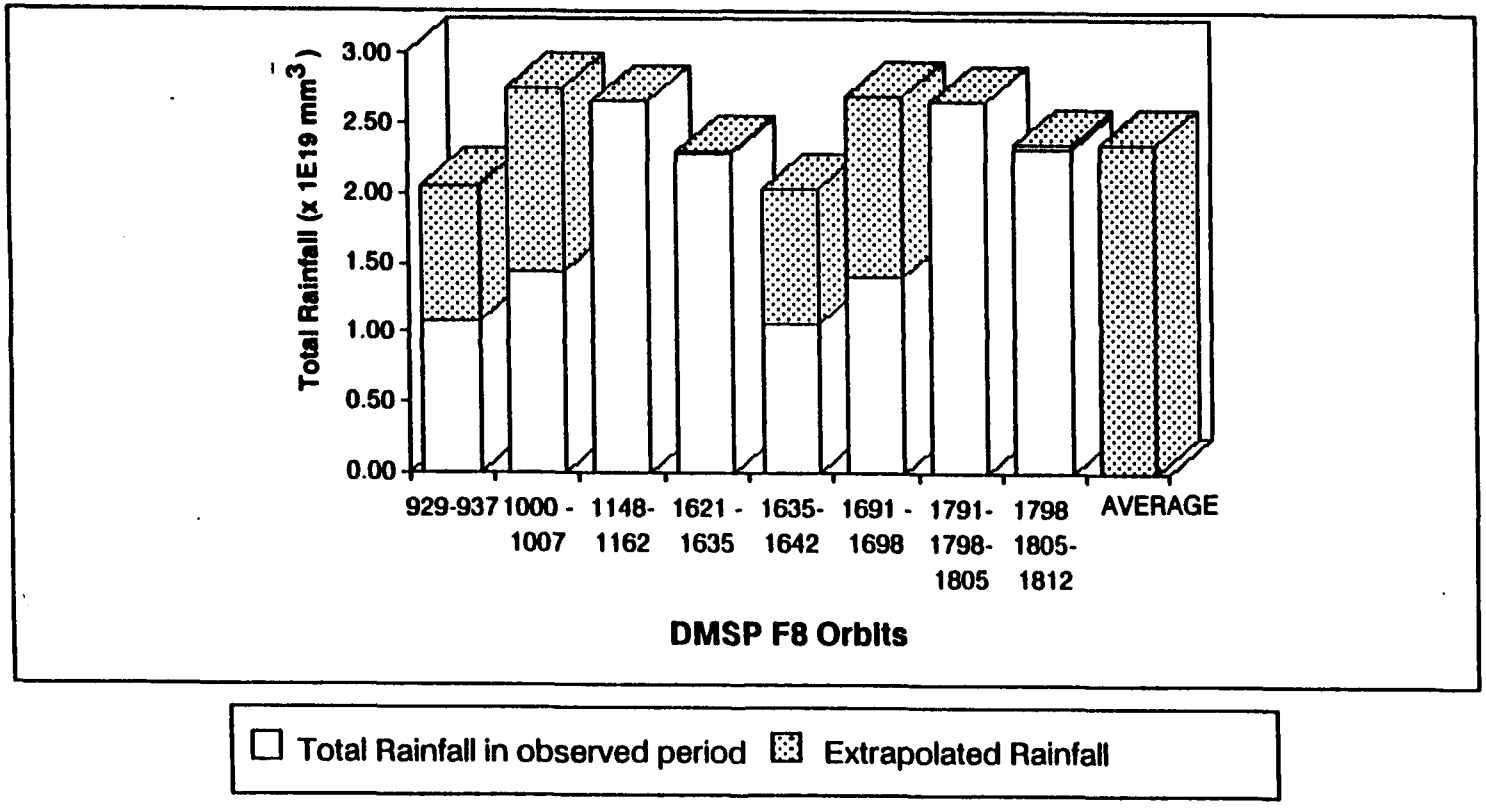

Fig. 5.4. Total 24 hour rainfall for eight typhoon cases. The total rainfall during the period was extrapolated to 24 hours if necessary.

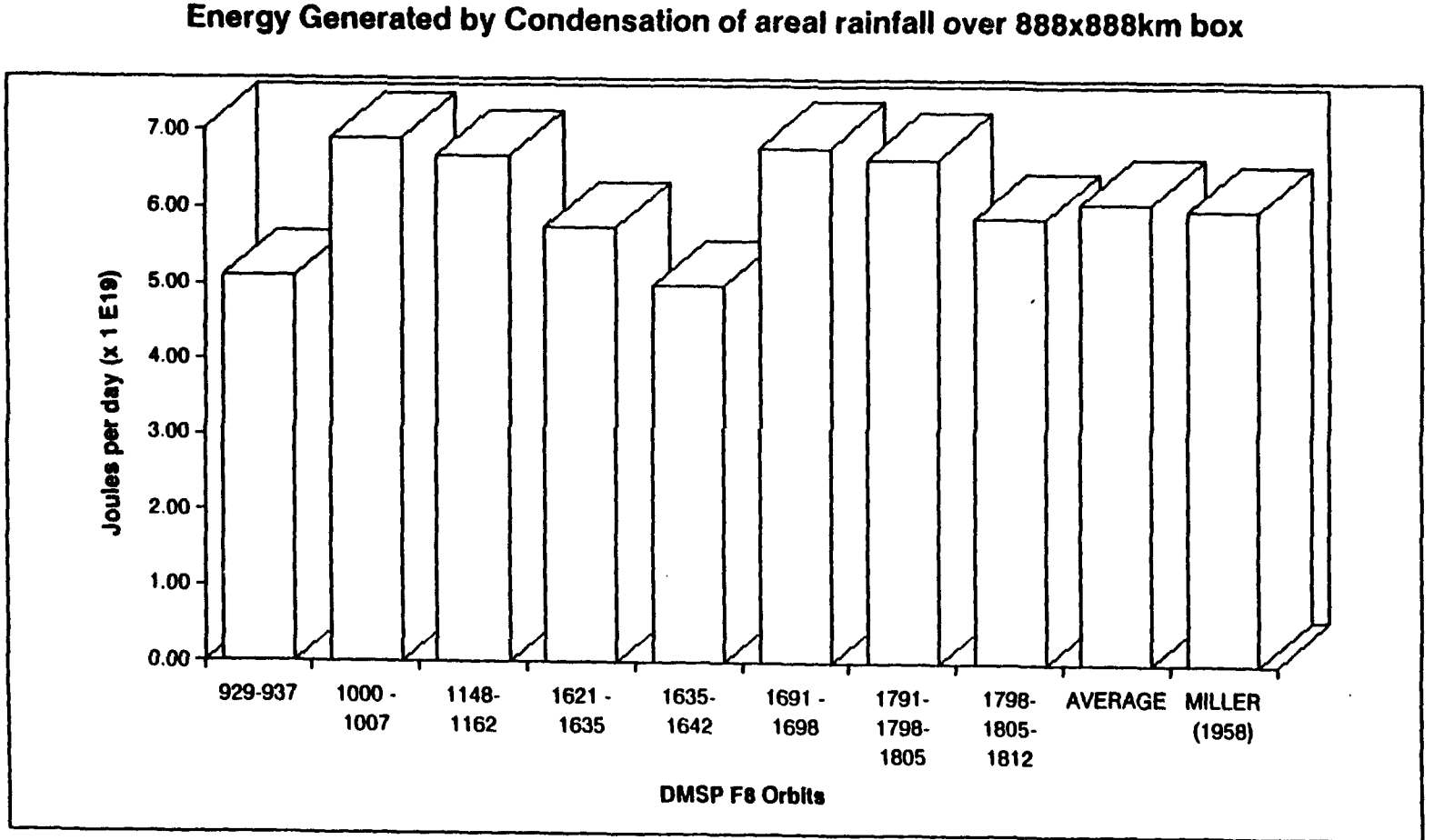

Fig. 5.5. Amount of latent heat generated by con-densation from total 24 hour rainfall for eight typhoon cases. The last column represents the results found by Miller(1958).

data for 16 Florida hurricanes. His grid was oriented along the direction of movement and rain amounts were averaged for all hurricanes prior to integration. Even though different data, SSM/I verses rain gauge, and a different methodology, the latent heat production values obtained using the SSM/I derived rainrates correspond well with previous calculations. Miller(1958) found an average latent heat production of 6.0×10^{19} Joules/day, a difference of only 1.7%.

There is some concern among reseachers with the large EFOV of the SSM/I and corresponding accuracies of retrieved rainrates. These results seem to indicate that although the SSM/I may underestimate large rainrates, when areal integration of the derived rainrates is performed, the effect of this beamfilling on total rainfall, may be minimized.

5.3 Sea Surface Temperature(SST) correlations

The original database consisted of 26 maptimes, however the database was reduced to 19 maptimes after it was screened for land contamination. The study required that tropical cyclones be over the open ocean regions in which the sea surface temperature grid (Fig. 5.3) encompassed only ocean regions. The individual maptimes are shown in Table 5.2.

Orbit	Tropical Cyclone	Date	Time (UTC)	Central Pressure (mb)	Intensity (knots)	Direction	Speed (knots)
506	Wynne	7/25/87	2200	972	65	300	11
788	Cary	8/14/87	2115	990	62.5	255	4
929	Dinah	8/24/87	2100	962.5	80	308	10
936	Dinah	8/25/87	930	945	105	318	10
1000	Dinah	8/29/87	2141	935	85	3	15
1007	Dinah	8/30/87	1009	938	85	22	19
1104	Holly	9/6/87	700	991	55	284	8
1105	Freda	9/6/87	900	992	57.5	75	3
1147	Holly	9/9/87	800	934	135	300	3
1161	Holly	9/10/87	800	911	130	78	6
1176	Freda	9/11/87	930	943	105	46	4
1416	Ian	9/28/87	930	970	72.5	95	1
1621	Kelly	9/12/87	2100	967.5	72.5	341	7
1635	Kelly	9/13/87	2050	965	80	342	11
1642	Kelly	9/14/87	930	965	82.5	320	11
1691	Lynn	10/17/87	2000	981	62.5	286	12
1698	Lynn	10/18/87	830	974	72.5	301	10
1748	Lynn	10/21/87	2100	938	107.5	255	15
2200	Nina	11/22/87	2100	962.5	82.5	260	16

Table 5.2. Typhoons and map times used in the correlation studies between areal sea surface temperature and their respective intensity and rainfall.

5.3.1 Mean Areal SST vs. Rainfall

In this portion of the study, the rainfall at the current maptime was correlated to sea surface temperatures in the region surrounding the tropical cyclone 24 hours earlier. The 24-h lag is thought to provide enough time for the air parcels in the periphery of the storm to pick up moisture and enter the core of the storm in the mid and lower levels. 222, 333 and 444 km boxes were used, since recent research by MacArthur(1991) identified that rainfall within this region could be related to future intensity.

Table 5.3 shows the correlation coefficients for the rainfall studies. The correlations between the total rainfall, total convective rainfall and the total stratiform rainfall were not as good as expected.

In all cases, correlations were relatively weak, i.e. < .5, with the maximum correlations found for SST's in the SE Quadrant versus 222 total and total convective rainfall (r=.44 and r=.42). The scattergram for the total rainfall regression(r=.44) is seen in Fig. 5.6. Total stratiform rainfall correlations were significantly less (.11).

Correlation between rainfall and Sea Surface Temperature

	NW	SW	NE	SE	Center	Outer	N. outer	S. outer	W. outer	E. outer
vs. 222 total	0.12	0.05	0.18	0.44	0.15	0.24	0.18	0.22	0.06	0.41
vs. 222 conv	0.12	0.10	0.05	0.42	0.10	0.16	0.12	0.18	0.04	0.32
vs 222strat	0.01	0.13	0.35	0.11	0.15	0.22	0.18	0.13	0.06	0.30
vs 333 total	0.18	0.05	0.01	0.42	0.01	0.27	0.13	0.34	0.20	0.28
vs 333 conv	0.21	0.01	0.08	0.41	0.02	0.21	0.11	0.27	0.17	0.23
vs 333 strat	0.01	0.16	0.16	0.14	0.01	0.22	0.08	0.27	0.13	0.22
vs 444 tot	0.23	0.13	0.12	0.31	0.05	0.24	0.09	0.35	0.26	0.15
vs 444 conv	0.29	0.11	0.12	0.34	0.01	0.25	0.13	0.32	0.27	0.16
vs 444 strat	0.37	0.03	0.27	0.10	0.37	0.18	0.35	0.05	0.14	0.20

Table 5.3. The correlation coefficients for total rainfall, total convective rainfall (conv) and total stratiform rainfall (strat) per hour as determined by SSM/I derived rainrates versus sea surface temperature areal means. 19 maptimes were used.

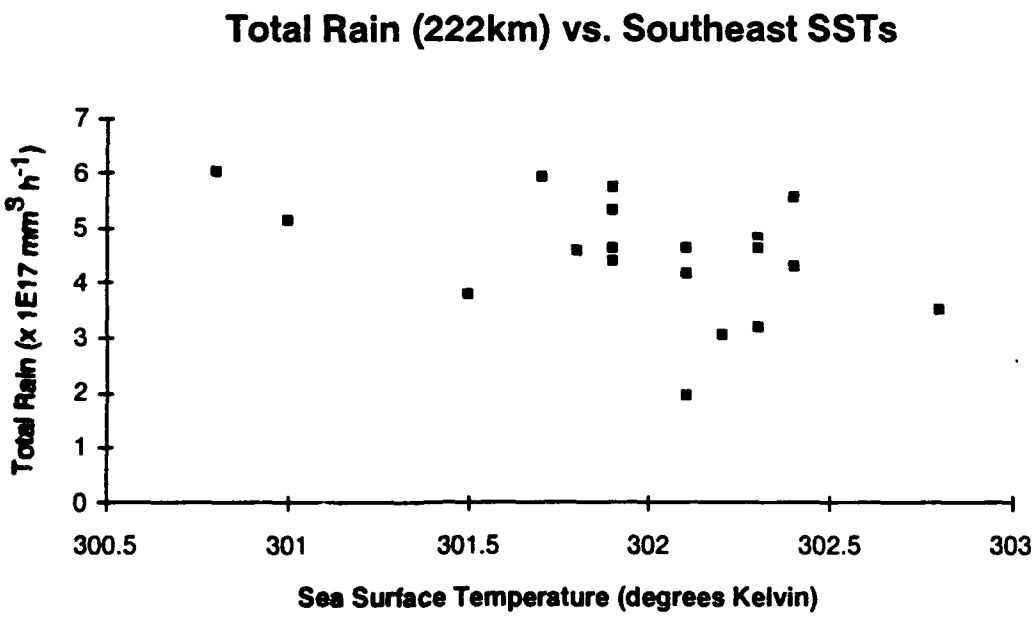

Fig. 5.6. Scatter diagram of total rainfall in 222km box as a function of sea surface temperature in the southeast quadrant. The line of best fit is represented by TR= -.974*SESST + 298.80; where SESST is in units of degrees Kelvin and TR in units of mm^3 h^{-1}.

In analyzing the data, there were no clear patterns or consistencies in the correlations, however it seemed that correlations were stronger for the total rain and convective rain. Although this study does not show a strong relationship between rainfall and sea surface temperature, it does shed some light on the problem

First, when performing a linear regression, the relationship is oversimplified, assuming a direct relationship between the two parameters. Previous work, such as Gray (1979), Ooyama(1982) and Merrill(1987) have mentioned numerous environmental factors effecting tropical cyclone maintenance and development. Those mentioned include the presence of mid level cyclonic vorticity, strong upper level outflow to act as an exhaust for the lower level convergence, conditional instability, ocean surface temperature and the depth of the warm water. Although SST's are important, as identified in climatological studies, it may be difficult to pinpoint their effect. In statistical prediction studies, Merrill(1987) supports the idea that tropical cyclones are influenced by innumerable environmental conditions, but suggests the individual relationships may appear weak when looked at by themselves.

5.3.2 SST Areal Variance versus Rainfall

In an attempt to further clarify the SST-Rainfall relationship, SST variance over the 10 regions were correlated against the rainfall.

In most cases, correlations improved but remained weak (<.5) (Table 5.4) At all three box radii, the strongest relationship was found for the total convective rainfall with a maximum coefficient of .48 for the 333km convective rainfall versus northwest and southwest region SST variance.

These results indicate that the convective rainfall may be dependent on the temperature contrast across the region, even if variances are only 1-2 degrees. This temperature contrast may initiate lower level instability similar to a midlatitude front.

It is important to note that these some SST variance may in fact be "caused" by the cloud cover from the convective system. The presence of clouds would contaminate the surface temperatures measured by the satellite, thereby contaminating the SST database used in this research. The degree of this contamination cannot be determined. Although current SST retrieval techniques have filters to determine

Correlation between rainfall and Sea Surface Temperature Variance

	NW var	SW var	NE var	SE var	Cen var	Out var	Nout var	Sout var	Wout var	Eout var
vs. 222 total	0.36	0.36	0.25	0.22	0.34	0.20	0.35	0.11	0.21	0.06
vs. 222 conv	0.40	0.40	0.19	0.28	0.37	0.22	0.37	0.13	0.24	0.09
vs 222strat	0.07	0.07	0.19	0.14	0.03	0.02	0.00	0.04	0.04	0.07
vs 333 total	0.41	0.41	0.18	0.17	0.34	0.26	0.39	0.23	0.29	0.03
vs 333 conv	0.48	0.48	0.20	0.30	0.42	0.29	0.44	0.23	0.31	0.08
vs 333 strat	0.04	0.04	0.02	0.23	0.07	0.01	0.00	0.07	0.03	0.25
vs 444 tot	0.36	0.36	0.08	0.16	0.27	0.20	0.32	0.20	0.23	0.05
vs 444 conv	0.45	0.45	0.12	0.29	0.38	0.26	0.40	0.22	0.28	0.08
vs 444 strat	0.02	0.02	0.09	0.14	0.06	0.01	0.01	0.09	0.01	0.21

Table 5.4. The correlation coefficients for total rainfall, total convective rainfall (conv) and total stratiform rainfall (strat) per hour as determined by SSM/I derived rainrates versus sea surface temperature areal variance. 19 maptimes were used.

cloud presence, final SST's can be expected to vary toward the colder in the presence of clouds.

5.4 SST Areal Means versus Future Intensity and Intensity Change

In this portion of the study, SST surrounding the tropical cyclone at the maptime were correlated against the intensity 12, 24, 36 and 48 hours following the maptime, i.e. the future intensity.

Correlations between the mean SST's and the various intensity parameters are shown in Table 5.5. As can be seen, there were moderate to strong correlations for all ten areas. Although correlations were good for all the areas, the strongest correlations were for the outer box, or the region surrounding the tropical cyclone. For example, the correlation coefficients for 24 and 48 hours were r=.66 and r=.81, respectively. Their scatter plots are shown in figures 5.7 and 5.8.

The results indicate a strong relationship between the SSTs and the future intensity. Figure 5.9 shows the correlation coefficients for the outer box as a function of time after the maptime. As the time interval increases, the correlation also increases. With the strongest correlations found between 24 and

Correlation Coefficients between intensity parameters and mean areal SST's

	NW	SW	NE	SE	Center	Outer	N. outer	S. outer	W. outer	E. outer
vs 12 h int	0.42	0.48	0.24	0.05	0.49	0.35	0.31	0.33	0.47	0.13
vs 12 h int ch	0.49	0.14	0.60	0.36	0.50	0.52	0.57	0.18	0.40	0.55
vs 24 h int	0.74	0.48	0.52	0.21	0.63	0.66	0.65	0.40	0.72	0.44
vs. 24 h int ch	0.62	0.12	0.61	0.34	0.44	0.62	0.67	0.21	0.51	0.60
vs 36 h int	0.79	0.51	0.59	0.44	0.64	0.77	0.73	0.54	0.80	0.58
vs 36 h int ch	0.57	0.18	0.52	0.43	0.38	0.59	0.61	0.30	0.51	0.58
vs 48 h int	0.79	0.44	0.61	0.58	0.61	0.81	0.77	0.57	0.79	0.66
vs 48 h int ch	0.55	0.13	0.53	0.54	0.37	0.60	0.61	0.34	0.49	0.62

Table 5.5. The correlation coefficients for 12, 24, 36 and 48 h intensities and intensity change versus mean areal sea surface temperature. 19 maptimes were used.

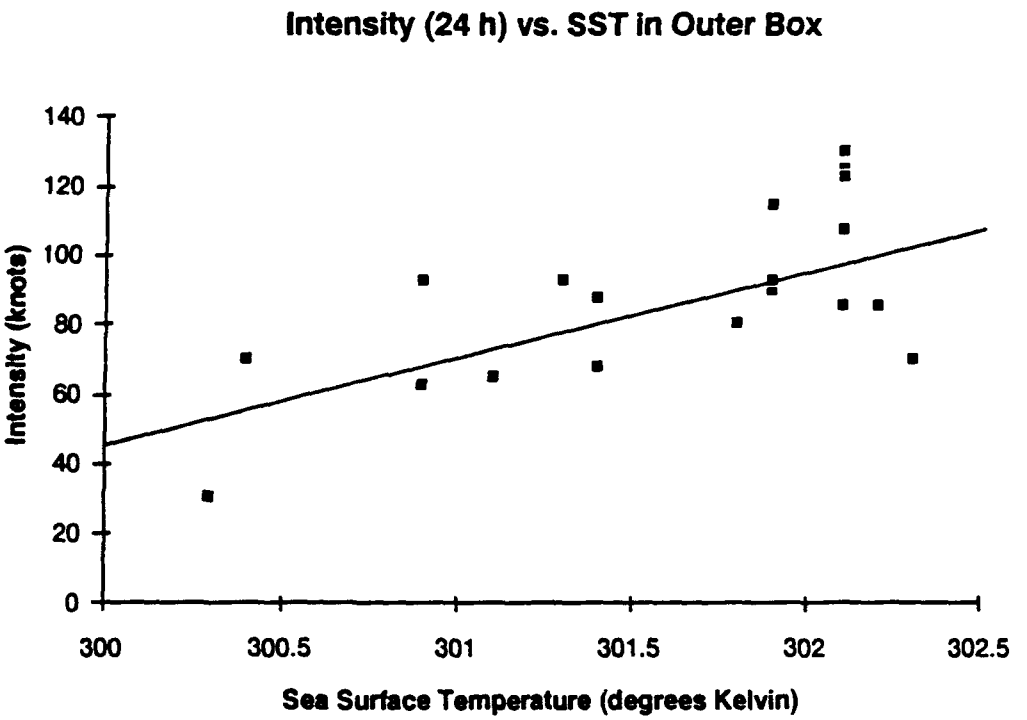

Fig. 5.7. Scatter diagram of 24 hour future intensity as a function of sea surface temperature in the outer box.
Linear fit data; INT24= 26.67*OUTSST - 7957.5; where OUTSST is in units of degrees Kelvin and INT24 in units of knots.

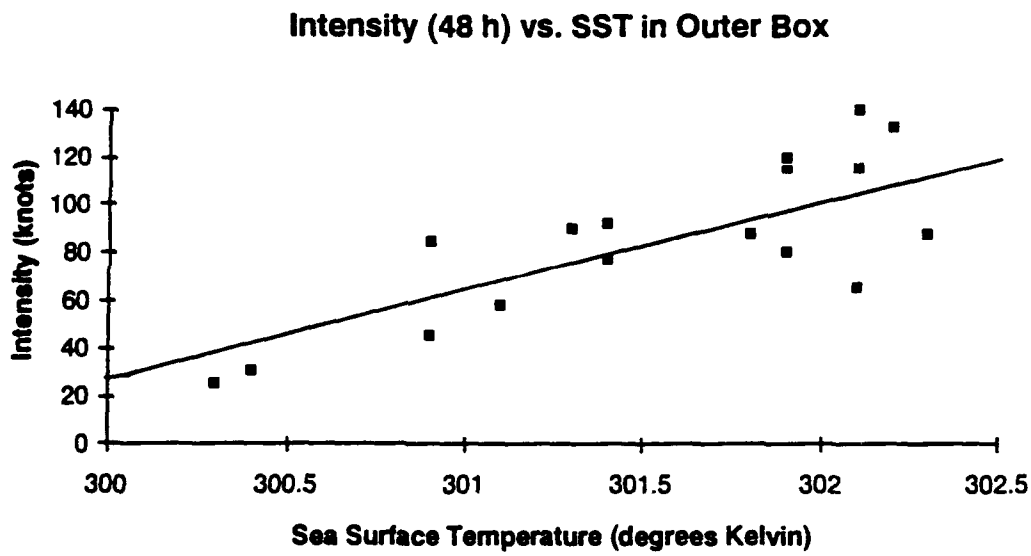

Fig. 5.8. Scatter diagram of 48 hour future intensity as a function of sea surface temperature in the outer box.
Linear fit data: INT48= 34*OUTSST - 10165.6; where OUTSST is in units of degrees Kelvin and INT24 in units of knots.

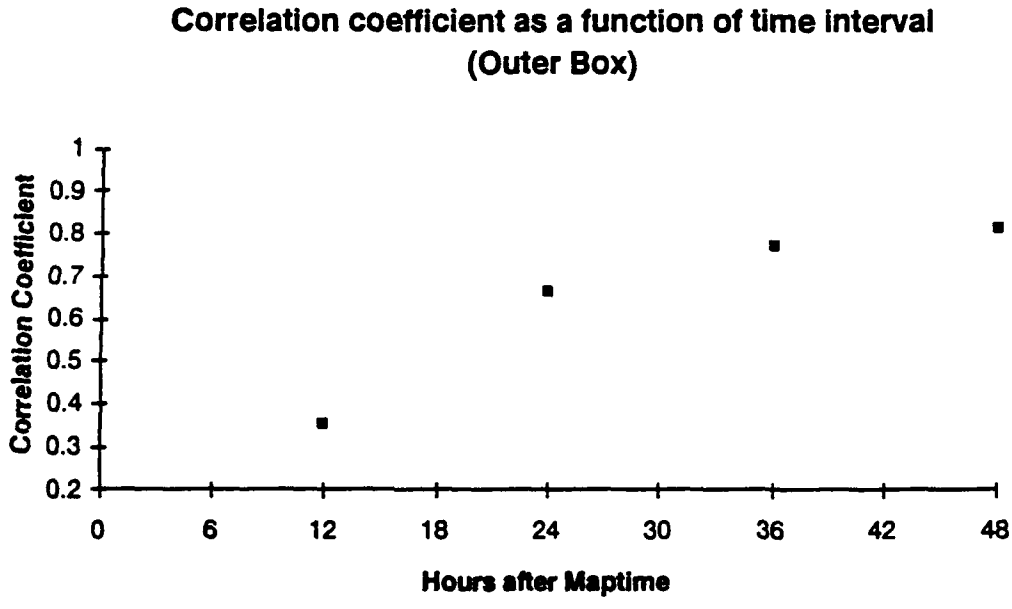

Fig. 5.9. Correlation coefficients for 12, 24, 36 and 48 hour future intensity as a function of sea surface temperatures in the outer box. Note that the correlation increases as the time from maptime increases.

48 hours, it is hypothesized that it takes 24-48 hours for the warm moist air to spiral inward with the cyclonic inflow to travel into the core of the tropical cyclone. Notice that 12 hour correlations are consistently weaker indicating that the storm is unable to transport the warmer air in that short of a time period. The correlation for the outer box improves 47% between 12 and 24 hours. The length of time for transport of the air parcels can be expected to vary according to the strength of the circulation, with more intense systems taking less time to transport the energy rich air into the center than weaker circulations.

The strong correlations for the 24-48 hour intensities correspond to the 1-2 day lag time between convective bursts and intensification as observed by Rodgers and Adler (1981), Steranka(1986) and MacArthur(1991). It seems apparent that the SST's in the region are a controlling mechanism in the transfer of sensible heat to the tropical cyclone system. This heat is used to pump up the system and increase convection, thereby increasing the intensity of the storm. Although this research does not show a direct relationship to rainfall, this may be due to other processes which govern precipitation processes, such

as lower level convergence and conditional instability. SST's may play an important role in the intensification process without a consequent increase in the observed rainfall.

Strong correlations were also observed between the SST and the intensity change, with the strongest correlations found between the SST's in the outer region and the intensity change over the next 24-48 hours (Table 5.4). Intensity change is obtained by subtracting the storm's intensity at maptime from the intensity at the time period of interest. The 24 hour scattergram is shown in Fig. 5.10. Regression coefficients for intensity and intensity change are shown in Table 5.6.

The regression equation for SST's in the outer region versus the 24-h intensity change is as follows:

$$24\text{hr intensity chg} = 23.0*\text{SST} - 6941.1$$

Using this equation, one can determine the critical temperature necessary for "status-quo" or development over the next 24 hours. By setting the 24-h hange to 0kts, the resultant SST is 301.5K or 28.3C. The 24 and 36 hour regression equations (Figs. 5.11 and 5.12) also yield critical temperatures of 28.3C and 28.6C, respectively, for continued

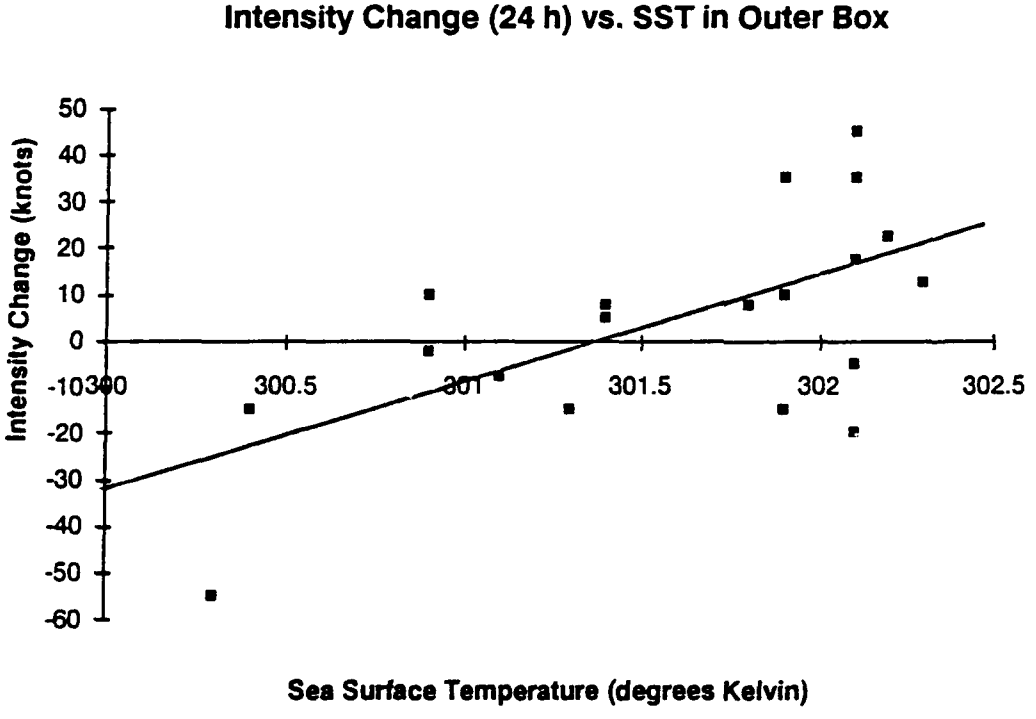

Fig. 5.10. Scatter diagram of 24 hour intensity change as a function of sea surface temperature in the outer box.
Linear fit data: CHG24=23.03*OUTSST - 6941.1; where OUTSST is in units of degrees Kelvin and CHG24 in units of knots.

Parameter	r	m	b	T*
24hr intensity	0.66	26.67	-7957.5	NA
36hr intensity	0.77	34.00	-10165.6	NA
48 hr intensity	0.81	42.68	-12784.6	NA
24 hr intensity change	0.52	23.03	-6941.1	301.5K (28.3C)
36 hr intensity change	0.62	30.35	-9149.2	301.5K (28.3C)
48 hr intensity change	0.59	39.00	-11768.3	301.8K (28.6C)

Table 5.6. Regression coefficients for correlations between sea surface temperatures in the outer box to various intensity parameters. Where **r** represents the correlation coefficient, **m**, the slope, **b**, the intercept, and **T***, the critical temperature necessary for development.

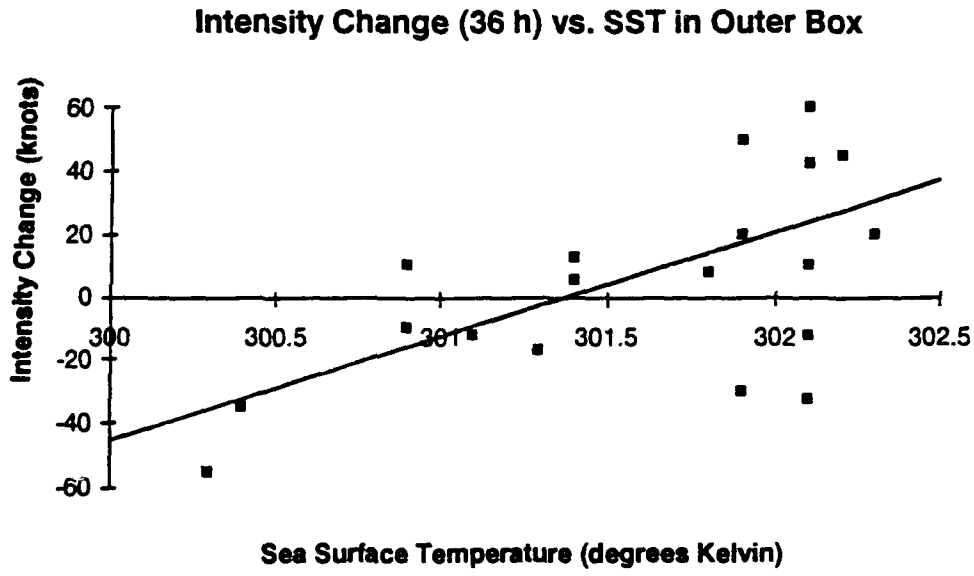

Fig. 5.11. Scatter diagram of 36 hour intensity change as a function of sea surface temperature in the outer box.
Linear fit data; CHG36=30.35*OUTSST - 9149.2; where OUTSST is in units of degrees Kelvin and CHG36 in units of knots.

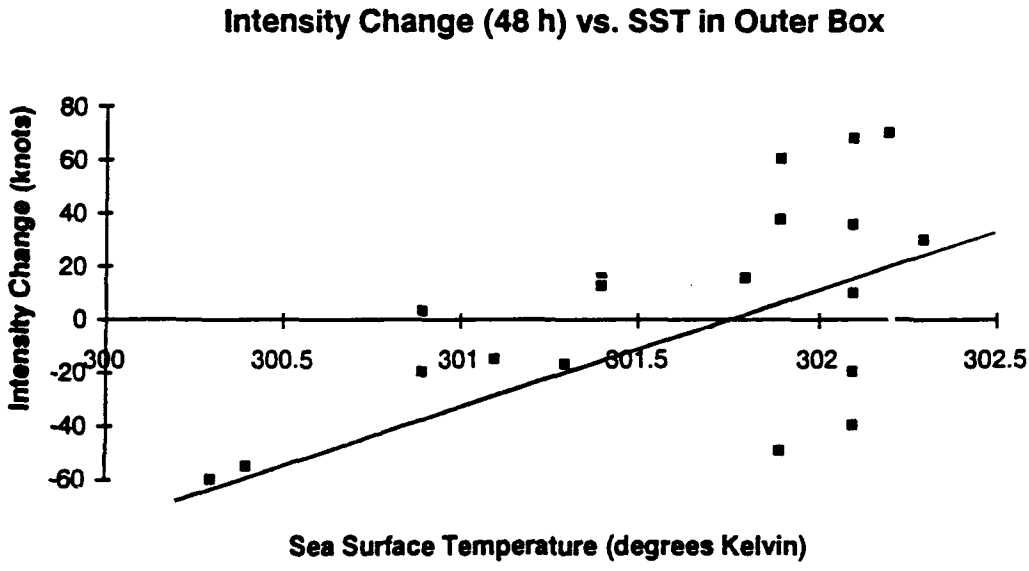

Fig. 5.12. Scatter diagram of 48 hour intensity change as a function of sea surface temperature in the outer box.
Linear fit data; CHG48=39*OUTSST - 11768.3; where OUTSST is in units of degrees Kelvin and CHG48 in units of knots.

development. This consistent result is noticeably higher than the climatological SST identified previously of 26.5C (Palmen, 1948; Gray, 1979). The 26.5C critical temperature was identified using climatology and focuses on identifying possible genesis regions and does not specifically refer to the continued development of an existing tropical cyclone.

Our results, in fact, are more in line with the 28.0C SST required for rapid deepening identified by Holliday and Thompson(1979). This difference may be attributed to the fact that the studies of Holliday and Thompson used climatological data and used the average temperature through a depth of 30m. Our SST data consists of observed ocean "skin" temperatures and would be expected to be higher than the 30m average temperature.

According to Dvorak (1984), the expected rate of development of a typhoon or hurricane is 25 knots per day. If intensification twice this rate is considered to be rapid develoment, the regression equation yields a necessary temperature of 303.6K or 30.4C.

Correlations were also strong for the northern regions, i.e., Northwest, Northeast, and North outer regions. Figure 5.13 represents a plot of the

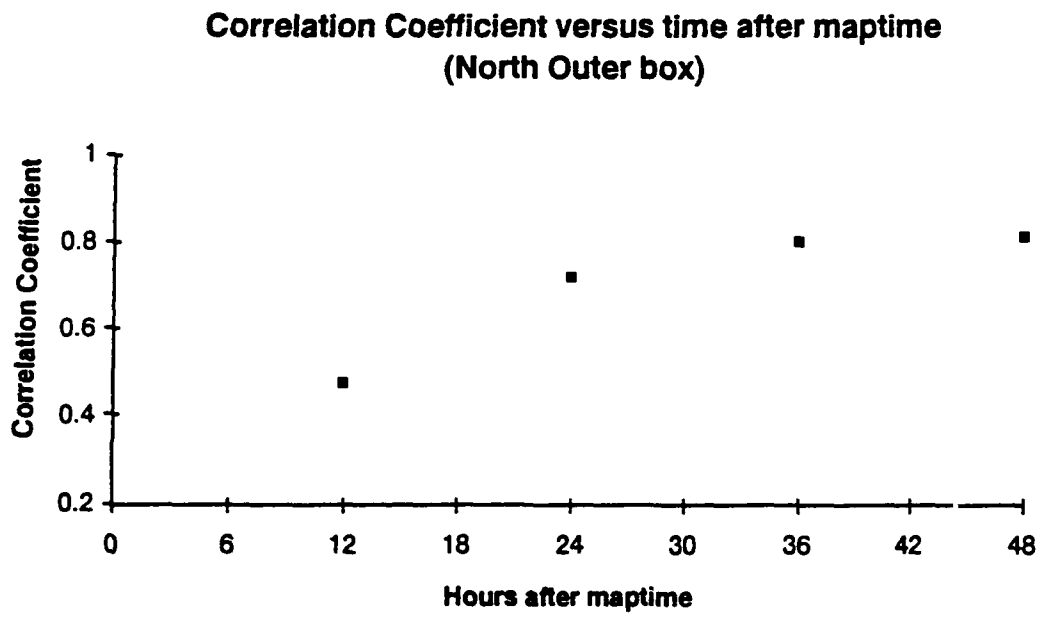

Fig. 5.13. Correlation coefficients for 12, 24, 36 and 48 hour future intensity as a function of sea surface temperatures in the north outer box. Note that the correlation increases as the time from maptime increases.

correlation coefficients at 12, 24, 36 and 48 hours for the north outer region. Strong correlations are also observed along with the same trend of increasing correlations with time as was found for the outer box and illustrated in Fig. 5.9.

This is not surprising as tropical cyclones typically weaken as they move north over the cooler temperatures. As one travels north in the North Western Pacific, SSTs lose a degree of their homogeneity with rapid decreases north of 30N latitude. Storms that move east to west over the open ocean tend to remain steady state or intensify as long as the upper level conditions remain favorable.

Several cases further illustrate these findings. Fig. 5.14 shows the SST distribution surrounding Typhoon Holly at 0700UTC 6 Sep 87. The temperatures are relatively uniform with all but a small portion to the east greater than 301.5K or 28.3C. Typhoon Holly developed over the next 24 hours with an increase in maximum sustained winds of 35 knots. This contrasts with that seen in Fig 5.15. This figure shows the SST distribution surrounding Holly four days later at 0800UTC 11 Sep 87. In this case, the SSTs to the north are significantly cooler than those seen in Fig 5.14. A strong temperature gradient is observed north

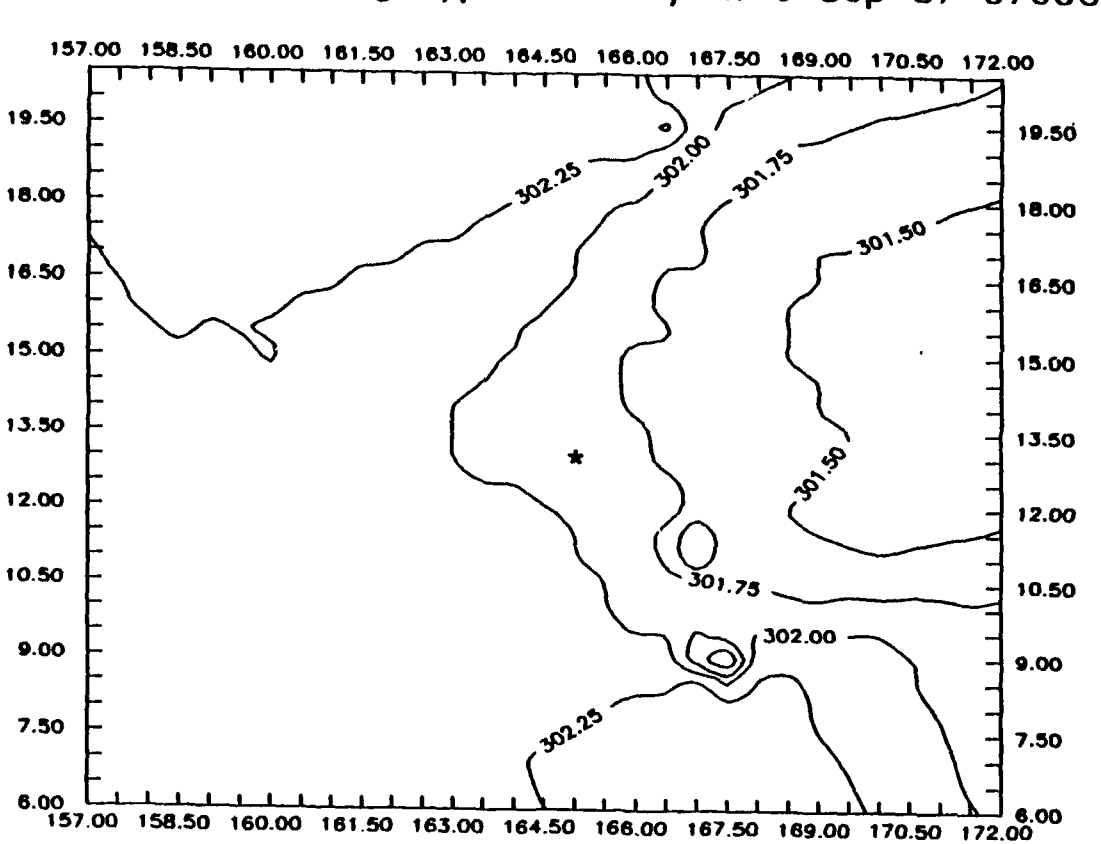

Fig. 5.14. Sea Surface Temperatures surrounding Typhoon Holly on 6 Sep 87 at 0700UTC. Note the temperatures are relatively uniform and greater than 301.5K or 28.3C. Holly intensified 35 knots in the next 24 hours. An asterisk shows Holly's position.

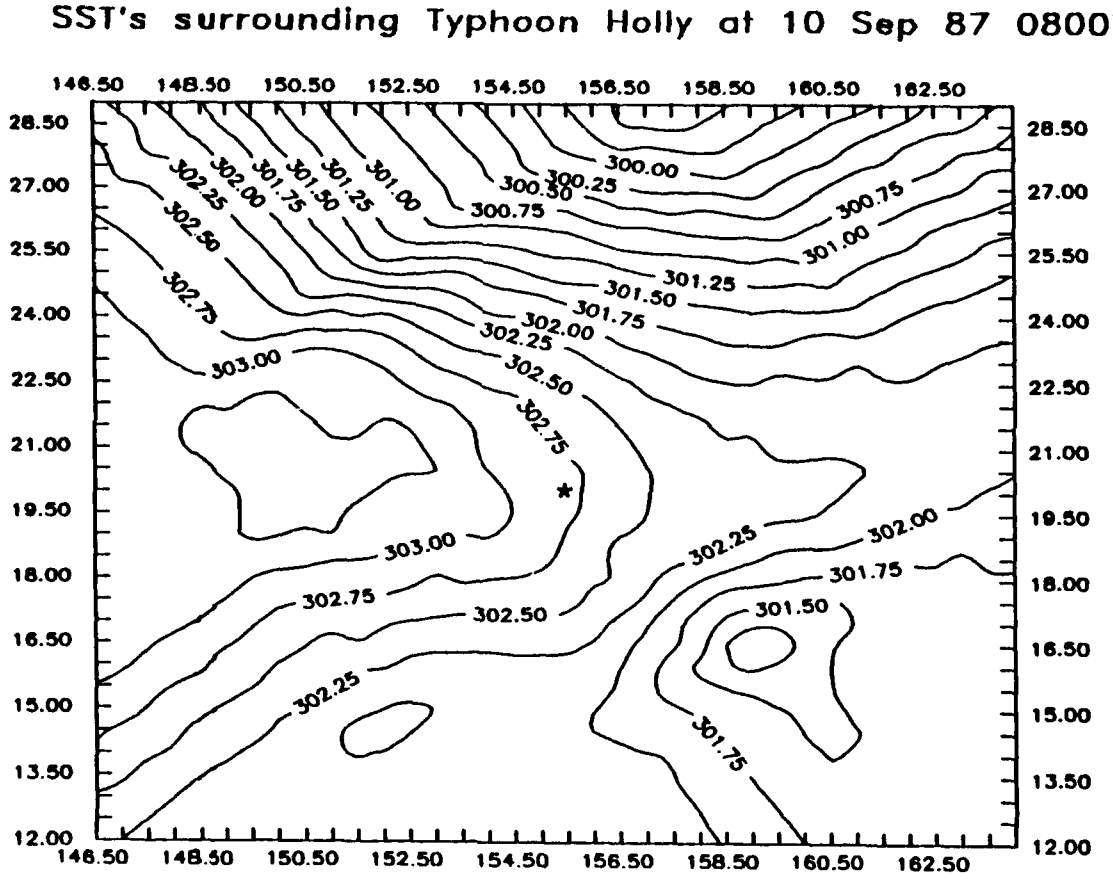

Fig. 5.15. Same as Fig. 5.14, except at 10 Sep 87 at 0800UTC. Note the significantly cooler temperatures north of 23 degrees North. Holly weakened by 15 knots in the next 24 hours. An asterisk denotes Holly's position.

of 23 degrees North with temperatures below 299.5K or 26.2C to the extreme north. During the 24 hours following, Holly weakened by 15 knots.

A similar response is seen in Figs 5.16 and 5.17. Fig. 5.16 represents the SSTs in the vicinity of Typhoon Freda at 0900UTC 6 Sept 87 and shows temperatures greater than 302K(or 28.8C). Typhoon Freda developed 12.5 knots over the next 24 hours. Five days later, Freda was surrounded by the surface temperatures seen in Fig. 5.17. In this figure, temperatures are noticeably cooler with a distinct cool pocket located to the east and southeast of the storm's center. Freda's maximum sustained winds weakened 20 knots over the next 24 hours.

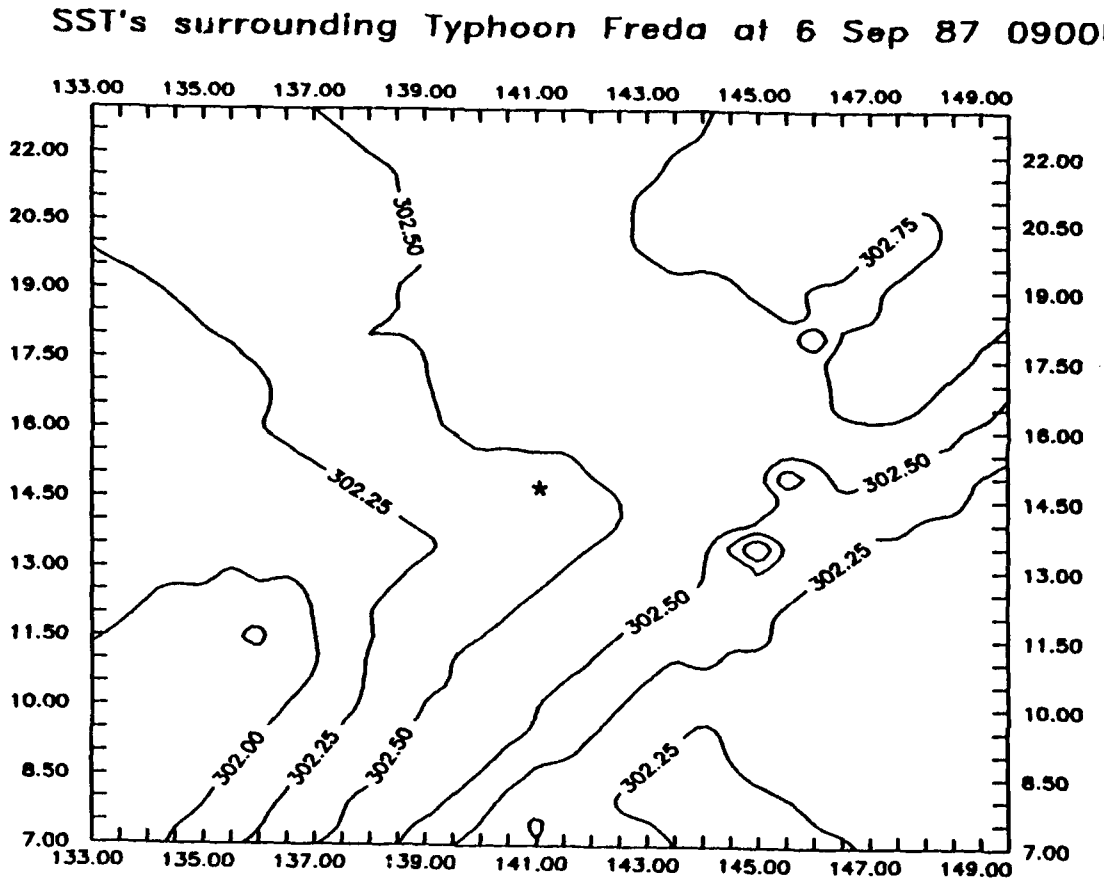

Fig. 5.16. Sea Surface Temperatures surrounding Typhoon Freda on 6 Sep 87 at 0900UTC. Note the temperatures are consistently greater than 302K (or 28.8C). Freda developed 12.5 knots over the next 24 hours. An asterisk denotes Freda's position.

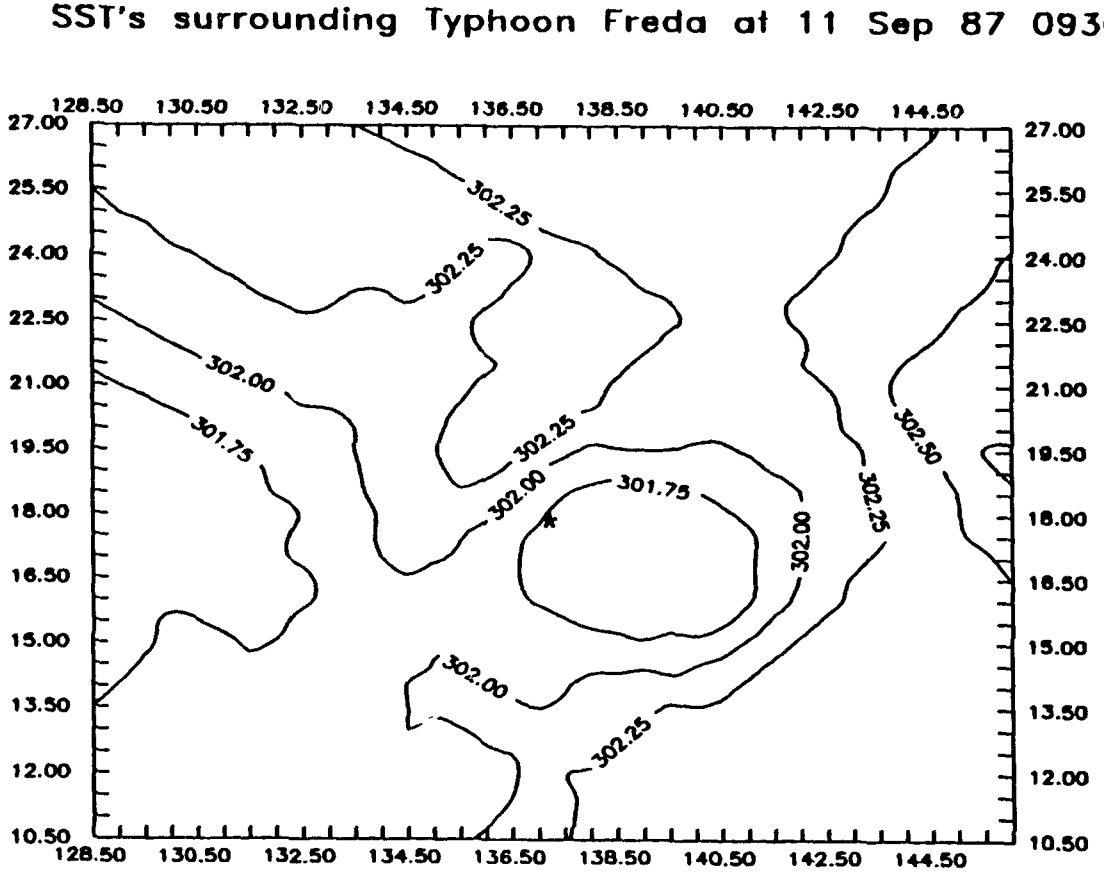

Fig. 5.17. Same as Fig. 5.16, except at 11 Sep 87 at 0930UTC. Notice temperatures are cooler in the region and there is a distinct cool pocket to the east and southeast of the storm's position. Freda's maximum winds weakened by 20 knots over the next 24 hours. An asterisk denotes Freda's position.

CHAPTER 6. SUMMARY AND CONCLUSIONS

Microwave data have proven useful in diagnosing the structure of the tropical cyclone and its environment. Specifically, the Special Sensor Microwave/Imager (SSM/I) mounted on the Defense Meteorological Satellite Program's F8 satellite provides new capabilities of studying their structure and processes.

This research used a nonlinear algorithm developed by Olson et al. (1989) to retrieve rainrates for tropical cyclones over tropical oceanic regions. These derived rainrates were used to determine the total 24-h rainfall and subsequent, amount of energy generated via latent heat release for eight cases. It was found that the average 24-h rainfall for the cases was 2.35 x 1E19 mm^3h^{-1}. This resulted in 6.1 x 10^{19} Joules generated per day via latent heat release during condensation.

These results are in good agreement with previous results and indicate that the SSM/I is a useful tool in estimating the total amount of rainfall of a tropical cyclone over oceanic regions. This information is critical as it will provide forecasters

the ability to predict the amount of rainfall expected as a tropical cyclone makes landfall and will allow for adequate disaster preparedness.

Because the rainrate footprint is relatively large, only the average rainrate is estimated. Thus, rainrate may be significantly less than those expected from a deep convective cell. However, our results showed that spatial averaging of these rainrates yielded total rain measurements in excellent agreement with those previously obtained using rain gauge observations. It seems possible, therefore, that underestimations of rainrates at smaller scales do not necessarily mean total rain over a larger area will be in proportionate error.

The rainrates were also used to study the effect of observed sea surface temperatures surrounding the storm to rainfall twenty four hours later. Our results indicate there is a only weak correlation between sea surface temperatures and the convective, stratiform and total rainfall. Although discouraging at first, the results support the conclusions of other researchers regarding the complexity of the tropical cyclone and the precipitation processes within it. These processes include the presence of convective forcing, such as low and midlevel convergence of the

horizontal winds and conditional instability. The degree of vertical development of the storm's clouds are also dependent on the storm's position relative to synoptic features, such as the tropical upper tropospheric trough and the subtropical ridge. Rainfall may be related to ocean temperatures, but this relationship is difficult to pinpoint using simple linear regression techniques.

Stronger correlations, although still less than 0.5, were found between the SST and rainfall. This indicates that the mesoscale temperature contrasts in the ocean surface may contribute to the development of precipitating clouds in a similar manner as in midlatitude frontal systems.

Significantly stronger relationships were identified between sea surface temperature and the lifecycle of the tropical cyclone in terms of intensity. Strong correlations were found between SST's surrounding the storm and the future intensity. The most significant relationship was found for the outer regions and the intensity 24-48 hours later. This 1-2 day lag repeatedly arises in other studies when referring to the lag between convective bursts and intensification and has been attributed to the time required for conversion of latent heat release to

kinetic energy. It seems apparent that SST's play a critical role in this process, although the specific mechanism is not known.

In addition, strong correlations were found between SST surrounding the storm and intensity change. Regression equations consistently yielded a critical temperature of 28.3-28.6C as necessary for the storm to remain steady-state or develop.

This research was limited by a smaller than desirable dataset. These relationships could be further examined with a larger database, and steps have been taken to increase this dataset. More work needs to be done concerning the relationships between the temperature contrast and the tropical cyclone, as microscale sea surface eddies may play a key role in tropical cyclone energetics and lifecycle.

REFERENCES

Adler, R.F., R.A. Mack, N. Prasad, H.-Y.M. Yeh, and I.M Hakkarinen, 1990: Aircraft microwave observationsand simulations of deep convection from 18 to 183 GHz. Part I: Observations. *J. Atmos Oceanic Technol.*, **7**, 377-391.

Anthes, R.A., 1982: Tropical Cyclones: Their Evolution, Structure and Effects. American Meteorological Society, Boston, MA., 208pp.

Burpee, R.W., and M.L. Black, 1989: Temporal and spatial variations of rainfall near the centers of two tropical cyclones. *Mon. Wea.Rev.*, **117**, 2204-2218.

Conway, R., 1989: SSM/I ascending nodal crossing data, Jun. 26 1987 through Aug. 13, 1989. Naval Research Laboratory, Washington D.C., 173 pp.

Dvorak, V.F., 1975: Tropical cyclone intensity analysis using satellite data. NOAA Tech. Rep NESDIS 11, Satellite Applications Laboratory, Washington, D.C., 47pp.

Emmanuel, K.A., 1986: An air-sea interaction theory for tropical cyclones. Part I: Steady-state maintenance. *J. Atmos. Sci.*, **43**, 585-604.

Felde, G.W. and M. Glass, 1989: SSM/I Brightness temperature analysis of tropical cyclones. Preprints. Fourth Conference on Satellite Meteorology and Oceanography, San Diego, CA., American Meteorological Society, Boston, MA., 400-404.

Frank, W.M., 1984: A composite analysis of the core of a mature hurricane. 984. *Mon. Wea. Rev.*, **112**, 2401-2420.

Gentry, R.C., E. Rodgers, J. Steranka, and W. Shenk, 1980: Predicting tropical storm intensity using satellite measured equivalentblackbody temperature of cloud tops. *Mon. Wea. Rev.*, **108**, 445-455.

Graves, C.E., 1992: Errors associated with microwave retrieval of rain: The Beamfilling Effect. Submitted to *J. Atmos. Oceanic Technol.*

Gray, W.M., 1968: Global view of the origin of the tropical disturbances and storms. Mon. Wea. Rev., **96**, 669-700.

Hoffman, C.W., V.G. Patterson, and D.J. McMorrow, 1987: Annual Tropical Cyclone Report. NAVOCEANCOMCEN /JTWC,Guam, U.S.A., 213pp.

Holliday, C.R., and Thompson, A.H., 1979: Climatological characteristics of rapidly intensifying typhoons. *Mon. Wea. Rev.*, **107**, 1022-1034.

Hollinger, J., R. Lo, G. Poe, R. Savage, and J. Pierce, 1987: Special Sensor Microwave Imager User's Guide. Naval Research Laboratory, Washington, D.C., 178pp.

Hollinger, J., 1991: DMSP Special Sensor Microwave Imager Calibration/Validation, Naval Research Laboratory, Washington D.C., **Volume II**, 11-1 - 11-40.

Jorgensen, D.P., 1984: Mesoscale and convective-scale characteristics of mature hurricanes. Part I: General observations by research aircraft. *J. Atmos. Sci.*, **41**, 1268-1285.

Kummerow, C., R.A. Mack, and I.M. Hakkarinen, 1989: A self-consistency approach to improve microwave rainfall rate estimation from space. *J. Appl. Meteor.*, **28**, 869-884.

Lee, T.F., and A. Caughey, 1989: Images of precipitation patterns associated with tropical cyclones using the SSM/I 85 GHz channel. Preprints. Fourth Conference on Satellite Meteorology and Oceanography, San Diego, CA., American Meteorological Society, Boston, MA., 45-48.

Liou, K.N., 1980: "An Introduction to Atmospheric Radiation." Academic Press, San Diego.

MacArthur, P.D., 1991: Microwave derived rainrates in typhoons and their use in the diagnosis and prediction of typhoon intensity., M.S. Thesis, St. Louis University, St. Louis, MO., available from University Microfilms, Ann Arbor, MI., 75 pp.

Merrill, R.T., 1988: Physical Retrieval of Typhoon Structure using Passive Microwave observations. Preprints. Fourth Conference on Satellite Meteorology and Oceanography, San Diego, CA., American Meteorological Society, Boston, MA., 405-408.

----------, 1988: Environmental influences on hurricane intensification. *J. Atmos Sci.*, **45**, 1678-1987.

----------, 1987: An experiment in statistical prediction of tropical cyclone intensity change. NOAA Tech. Memo. NWS NHC 34, 34pp.

Miller, B.I., 1958: Rainfall rates in Florida hurricanes. *Mon. Wea. Rev.*, **86**, 258-264.

Olson, W.S., F.J. Fontaine, W.L. Smith, and T.H. Achtor, 1990: Recommended algorithms for the retrieval of rainfall rates in the tropics using SSM/I (DMSP-8). Manuscript, Univ. of Wisconsin, Madison. 10pp.

Olson, W.S., 1989: Physical retrieval of rainfall rates over the ocean by multispectral microwave radiometry: Application to tropical cyclones. *J. Geophys. Res.*, **94**, 2267-2280.

Ooyama, K.V., 1969: Numerical Simulation of the lifecycle of tropical cyclones. *J. Atmos. Sci.*, **26**, 3-40.

Palmen, E., 1948: On the formation and structure of tropical hurricanes. *Geophysica*, **3**, 26-38.

Powell, M.D., 1990: Boundary layer structure and dynamics in outer hurricane rainbands. Part I: Mesoscale rainfall and kinematic structure. *Mon. Wea. Rev.*, **118**, 891-917.

Rao, G.V., P.D. MacArthur, and J.H. McCoy, 1991: The SSM/I latent heat release and brightness temperature anomalies associated with tropical cyclones and their utility in predicting the intensity changes of tropical storms. Preprint. Fifth Conference on Satellite Meteorology and Oceanography, San Diego, CA., American Meteorological Society, Boston, MA., 175-178.

Rappaport, E.N., 1991: Operational Applications of SSM/I data at the National Hurricane Center. Preprint. Fifth Conference on Satellite Meteorology and Oceanography, American Meteorological Society, Boston, MA., 179-183.

Rodgers, E.B., and R.F. Adler, 1981: Tropical cyclone rainfall characteristics as determined from a satellite passive microwave radiometer. *Mon. Wea. Rev.*, **109**, 506-521.

Sadler, J.C., 1976: A role of the tropical upper tropospheric trough in early season typhoon development. *Mon. Wea. Rev.*, **104**, 1266-1278.

Spencer, R.W., H.M. Goodman, and R.E. Hood, 1989: Precipitation retrieval over land and ocean with the SSM/I: Identification and characteristics of the scattering signal. *J. Atmos. Oceanic Technol.*, **6**, 254-273.

Spencer, R.W., and R.E. Hood, 1989: SSM/I liquid and frozen precipitation patterns in Hurricane Gilbert. Preprints. Fourth Conference on Satellite Meteorology and Oceanography, San Diego, CA., American Meteorological Society, Boston, MA., 86-89.

Steranka, J., E.B. Rodgers, and R.C. Gentry, 1986: The relationship between satellite measured convective bursts and tropical cyclone intensification. *Mon. Wea. Rev.*, **114**, 1539-1546.

USAFETAC Climatic Database. User's Handbook No. 2, 1986: Surface Temperature Analysis. USAF Environmental Technical Applications Center, OL-A, Asheville, NC.

Velden, C.S., W.S. Olson, and B.A. Roth, 1989: Tropical cyclone center-fixing using DMSP SSM/I data. Preprints. Fourth Conference on Satellite Meteorology and Oceanography, San Diego, CA., American Meteorological Society, Boston, MA., J36-J39.

Willoughby, H.E., 1988: The dynamics of the tropical cyclone core. *Aust. Met. Mag.*, **36**, 183-191.

BIOGRAPHY OF THE AUTHOR

Timothy David Hutchison was born on December 30, 1961 in St. Louis, Missouri. He graduated from St. Louis University High School in 1980. In 1983, he graduated from Trinity University in San Antonio, Texas, receiving a Bachelor of Arts degree in Chemistry and Biology. In 1985, he graduated from the United States Air Force Officer Training School in San Antonio and received his commission. After his commision, he studied Meteorology for one year at San Jose State University, California through the Air Force Institute of Technology(AFIT). From 1986 to 1988, he served as the Wing Weather Officer to the 19th Air Refueling Wing at Robins Air Force Base, Georgia. In 1988, he was assigned to Detachment 1, First Weather Wing at Nimitz Hill, Guam, where he served as the Meteorological Satellite Coordinator and Officer in Charge of the Commander in Chief Pacific Forces (CINCPAC) Satellite Network for the Joint Typhoon Warning Center. In 1990, he returned to AFIT where he began a Master's program in Meteorology at St. Louis University, Missouri. He is married to the former Koryn Renae Beltz. They have three sons, Kyle, Curtis and Keith.